

Review

Microwave-Assisted Synthesis as a Promising Tool for the Preparation of Materials Containing Defective Carbon Nanostructures: Implications on Properties and Applications

Damian Pawelski and Marta E. Plonska-Brzezinska * 

Department of Organic Chemistry, Faculty of Pharmacy with the Division of Laboratory Medicine, Medical University of Białystok, Mickiewicza 2A, 15-222 Białystok, Poland; damian.pawelski@sd.umb.edu.pl

* Correspondence: marta.plonska-brzezinska@umb.edu.pl

Abstract: In this review, we focus on a small section of the literature that deals with the materials containing pristine defective carbon nanostructures (CNs) and those incorporated into the larger systems containing carbon atoms, heteroatoms, and inorganic components. Briefly, we discuss only those topics that focus on structural defects related to introducing perturbation into the surface topology of the ideal lattice structure. The disorder in the crystal structure may vary in character, size, and location, which significantly modifies the physical and chemical properties of CNs or their hybrid combination. We focus mainly on the method using microwave (MW) irradiation, which is a powerful tool for synthesizing and modifying carbon-based solid materials due to its simplicity, the possibility of conducting the reaction in solvents and solid phases, and the presence of components of different chemical natures. Herein, we will emphasize the advantages of synthesis using MW-assisted heating and indicate the influence of the structure of the obtained materials on their physical and chemical properties. It is the first review paper that comprehensively summarizes research in the context of using MW-assisted heating to modify the structure of CNs, paying attention to its remarkable universality and simplicity. In the final part, we emphasize the role of MW-assisted heating in creating defects in CNs and the implications in designing their properties and applications. The presented review is a valuable source summarizing the achievements of scientists in this area of research.

Keywords: carbon nanostructure; defect; heteroatom doping; catalysis; electrocatalysis; electrochemistry; supercapacitor; microwave irradiation; microwave-assisted synthesis; inorganic nanoparticle



check for updates

Citation: Pawelski, D.; Plonska-Brzezinska, M.E. Microwave-Assisted Synthesis as a Promising Tool for the Preparation of Materials Containing Defective Carbon Nanostructures: Implications on Properties and Applications. *Materials* **2023**, *16*, 6549. <https://doi.org/10.3390/ma16196549>

Academic Editors: Sergei A. Kulnich, Valery A. Svetlichnyi and Neli Mintcheva

Received: 1 August 2023

Revised: 27 September 2023

Accepted: 29 September 2023

Published: 4 October 2023



Copyright: © 2023 by the authors. Licensee MDPI, Basel, Switzerland. This article is an open access article distributed under the terms and conditions of the Creative Commons Attribution (CC BY) license (<https://creativecommons.org/licenses/by/4.0/>).

1. Introduction

The term “nanoscale” is applied to objects up to 100 nm in size. It also applies to structures built of many atoms, forming groups called nanostructures because their size falls within this scale. These consist mainly of carbon atoms (carbon nanostructures, CNs), whose combination in well-organized macromolecular systems creates structures with unique properties, and they are among the most popular in this group [1–3]. Different morphological variations of CNs, for example, nanocones [4], nanotubes [5], diamond-like carbon [6,7], onion-like carbon [8], nanofibers [4], graphene [9], and graphdiyne [10–12], have become quite well known [4,8,9,13,14]. Despite almost identical chemical compositions, the CNs differ significantly in their physical properties with different dimensionality and chemical reactivity [3,15]. These greatly affect their subsequent use in many areas, mainly in electronics [16,17], catalysis [18,19], electrocatalysis [20], energy conversion and storage [21–23], sensors [24–28], and for biomedical [29], biological, and environmental applications [30–33]. The electrochemical and electrocatalytic properties of carbon-based materials are closely related to their chemical composition and structure [34–36]. CNs are characterized by excellent conductivity and mechanical stability, large specific areas (active surface) with micro- and mesoporosity, and high mobility of the charged carrier [37–40],

which only strengthens their position in the abovementioned areas. CNs can be easily modified by producing numerous defective motifs, shortly called defects, with different chemical characters that enhance the physicochemical properties of the materials. Defects in nanomaterials are considered ‘active sites’ of the reaction because they change the electron density in the material, affecting the electronic and surface properties in the local region [41–43]. As for photocatalysis [44,45] and electrocatalysis [46–48], reactions occur on the contact interface between ‘active sites’ of materials and reactive species. The defects modify the electronic structure of the CNs, simultaneously affecting the chemisorption of the key reaction intermediates [41]. This process enhances the reaction kinetics, consequently increasing electrocatalytic efficiency [49,50]. In terms of energy-storage devices, carbon-based materials are generally used as electrodes in electrochemical capacitors [35,51,52]. The energy storage mechanism in supercapacitors (SCs) is based on reversible ion adsorption on a high specific surface area (SSA) of porous carbon materials at the carbon/electrolyte interface [53]. It was also found that defects in sp^2 -hybridized CNs significantly improved ion storage performance [54]. Thus, the contact area at the interface is crucial for efficient electrocatalytic reactions and electrochemical storage devices.

Structural defects can be of various natures and can be introduced into the “ordered” structure during the formation of CNs or as a result of post-modification processes. Direct methods for producing defective CNs (d-CNs) include chemical vapor deposition (CVD) [55–57], thermal treatment [58,59], pyrolysis [60,61], microwave (MW) irradiation [62–65], etc. Using different process parameters and substrates, it is possible to produce pristine d-CNs or more complex systems containing, for example, heteroatomic dopants or inorganic components [66–69]. A post-modification process is often also used, which leads to introducing external defects into the CN’s surface. It is used as one stage of the carbon-based materials production processes or to modify the already formed CNs. The latter case is frequently connected with chemical treatment, which uncontrollably introduces defects in the outer layers of CNs with the simultaneous creation of functional groups on the nanostructure’s surface due to the redox reaction of the C atoms of the outer carbon layer [48,70–73]. CNs can be modified in more controllable manner using, for example, plasma-induced functionalization [74,75] or MW irradiation [76,77]. In these cases, the concentration of topological defects introducing functional groups or heteroatom dopants can be controlled by the appropriate selection of process parameters.

All these aspects will be discussed in more detail in our review. We decided to discuss the literature related to MW-assisted synthesis used in the creation of d-CNs due to its simplicity, its economy, and the possibility of conducting the reaction in solvents and solid phases in the presence of components of different chemical natures, which allows the use of them in various combinations. It is the first literature review that deals with the use of MW-assisted heating to modify the structure of CNs, which are aimed at introducing topological changes that, consequently, modify their physical and chemical properties and, therefore, decide on their further application. This review focuses on the materials containing pristine d-CNs and those incorporated in the hybrid materials. We will emphasize the advantages of synthesis using MW-assisted heating and the implications for the chemical and physical properties of CNs. In the final part of the work, we present examples of the use of MW-assisted heating to obtain materials that have promising properties and can be used in electrochemistry and electrocatalysis.

2. Defects and Their Structural Variation

Defects can be divided into four categories based on their size and location [41,78–80]:

1. Zero-dimensional (0D) point defects (e.g., doping, vacancy, reconstruction), which can be further divided into reconstructed or vacancy defects, non-metallic-atom-doping induced defects, and metal defects [42,81].
2. One-dimensional (1D) line defects (e.g., dislocation).
3. Two-dimensional (2D) planar defects (e.g., grain boundary).
4. Three-dimensional (3D) volume defects (e.g., spatial lattice disorder).

The disorder in the crystal structure is related to the ideal lattice structure [82,83]. In 2D materials, such as graphene, the types of defects are very diverse [84]. Point defects are on a tiny scale, referring even to the defect of a single atom in the crystal. Due to the location of this defect, we distinguish among them vacancy, dislocation, interstitial defect, replacement, and antisite. Line defects are related to disturbances in the crystal structure along the crystalline (for example, grain boundaries). Surface defects have a very diverse nature. It is defined as any disturbance of the crystal structure in one direction. Here, we can indicate, for example, twin crystals, grain boundary, hole, etc. The last group of defects, the largest in their scale, are defects related to 3D structure.

In electrochemistry, where reactions occur on the electrode surface, the electrode materials can be considered basal and non-basal surfaces. Carbonaceous materials, including graphene and graphite derivatives, are used as electrode materials, with ideal model structures for studying electrochemical processes. We can distinguish basal and non-basal surfaces in both systems, including edge surfaces and defect surfaces [85]. The ideal basal surfaces are considered a well-organized layer of only six-ring carbons. The presence of pentagonal and heptagonal rings, pentagon–heptagon pairs, and occasional quadrangular and octagonal ones in the graphene layer is defined as in-plane topological defects (non-basal surfaces) [86].

The combination of tightly bounded pentagons and neighboring heptagons (Stone–Wales (SW) defect) can be identified as an edge dislocation in a 2D hexagonal lattice (Figure 1a) [87]. The SW defects are created by rotating a C–C bond, transforming the four adjacent hexagons into two pentagons and two heptagons [88]. If the SW defect is separated through hexagonal units into two separate pentagon–heptagon connections, dislocation dipoles (DD_n) appear in the graphene structure. The subscript n indicates the distance between two 5–7 pairs in the hexagon units (distance l , Figure 1b–f). DDs are not only in-plane surface defects but also cause out-of-plane ring deviation due to introducing irregular defects into the graphene layer (height h , Figure 1c–f).

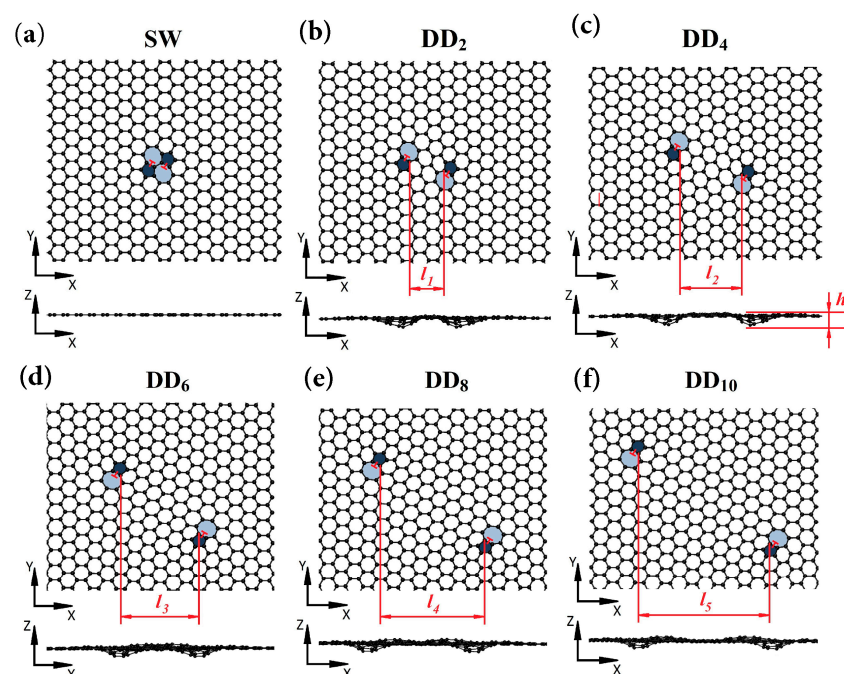


Figure 1. Typical structures of graphene in two projections: (a) graphene with SW defect, (b–f) graphene with dislocation dipole (DD_n) with the different arm, the subscript n indicates the distance between two 5–7 pairs in the hexagon units. Pentagons and heptagons are colored in dark and light blue, respectively. Geometrical parameters for dipoles, values of dipole arm (l) and buckling height (h) for graphene with the following defects: SW ($l = 0$; $h = 0$); DD_2 ($l = 6 \text{ \AA}$; $h = 1.89 \text{ \AA}$); DD_4 ($l = 11 \text{ \AA}$; $h = 2.0 \text{ \AA}$); DD_6

($l = 15 \text{ \AA}$; $h = 1.25 \text{ \AA}$); DD₈ ($l = 20 \text{ \AA}$; $h = 1.22 \text{ \AA}$); DD₁₀ ($l = 25 \text{ \AA}$; $h = 1.78 \text{ \AA}$) Reprinted with the permission from MDPI, Ref. [88].

The differentiation of defects is also introduced, considering materials' physical and chemical properties. Here, we can distinguish Frenkel defects (interstitial atoms) [89], Schottky defects (carbon vacancies) [89], heteroatom-doping (doping defects) [66], electronic defects in the crystal [90], and nonstoichiometric structured defects [91], etc. No matter how the structural defects in CNs are subdivided, they refer to some disturbance of the structure compared to the 'ideal structure' of the nanomaterials. This 'disturbance' changes some specific features of the nascent nanostructure, consequently modifying the physical and chemical properties of the CNs.

3. Heteroatom Doping and Structural Defects of CNs with Relevance in Electrocatalysis and Electrochemistry

Carbon materials act as a catalyst or materials with satisfactory electrochemical or electrocatalytic performance. However, amorphous or disordered carbon materials exhibit low activity, chemical, thermal and electrochemical stability, and low oxidation resistance [92–94]. The combination of carbon atoms in a 2D or 3D manner increases its stability, and at the same time, an organized macromolecular architecture defines its physical and chemical properties.

Carbon materials used as electrodes in capacitors show a direct relationship between the electrostatic capacitance and their SSA values [95]. However, nanoscale systems do not directly comply with the above rule. In this case, the nanoscale and quantum effects must be frequently considered because it has a large surface-to-volume ratio. In this case, we observe an increased role of the material's surface in the capacitive storage process [96]. It is essential to not only the total number of pores but also their size and arrangement of pores. Carbon defects of various natures, such as dislocations, atomic vacancies, and stacking faults, comprise the surface active regions (ASA) in catalytic/electrocatalytic reactions [97] or SSA in electrochemistry. The whole is a structural feature of graphitic CNs [98]. Several experimental and theoretical studies have shown that the experimental conditions during the creation of defects influence the CNs' ASA and SSA [55,98].

Microstructural variations of CNs are also strongly connected with their conductivity and field emission. High-performance field emission (FE) requires low turn-on and threshold fields, good electrical and mechanical stability, and dense and uniform emission sites [99]. The carbon nanotubes (CNTs) with excellent conductivity meet the abovementioned criteria. In Figure 2b,d, on the transmission electron microscopic (TEM) images, the influence of the MW-assisted H₂ plasma process on the structural changes of the CNs is presented. The thinned and open-ended caps of the CNTs can yield larger FE. Raman spectroscopy enabled a qualitative assessment of the created CNs by comparing the intensity of the starting material's D- and G-bands (I_D/I_G) and those subjected to plasma treatment. Increasing the I_D/I_G ratio with MW irradiation time indicates the formation of defects in the structure of CNTs. The created sp³-hybridized defects (defected graphite) on the CNT's walls may act as new emission sites [100–102]. Plasma treatment also reduces the number of graphene layers and cup openings in CNTs (Figure 2b–d) [99]. Open-ended CNTs can facilitate electron tunneling and significantly improve the physical parameters of d-CNTs. The most significant is the high emission current density of 10.36 mA/cm². In summary, MW irradiation and H₂ plasma processing increase electron transferring traces and enhance CNT's FE performance.

The studies confirmed that defects in graphitized carbons at the nanoscale significantly enhance the electrochemical behavior in aqueous electrolytes. For example, the use of 'small' spherical nanostructures (Figure 3a), called carbon nano-onions (CNOs) in energy storage devices, has enabled high power and high energy [103]. Comparing the CNO parameters to conventional carbon black and graphite nanoparticles in these devices allows for better gravimetric and volumetric parameters [1,103]. For example, CNOs obtained from nanodiamond (ND) particles at 1800 °C showed a high SSA, determined using the

Brunauer–Emmett–Teller theory (S_{BET}), of about $680 \text{ m}^2/\text{g}$ [104], lower than that of many carbon materials [105–107]. Despite this, the external surface is fully available for the adsorption of ions from the solution, which allows for achieving optimal parameters of devices accumulating an electric charge [108,109].

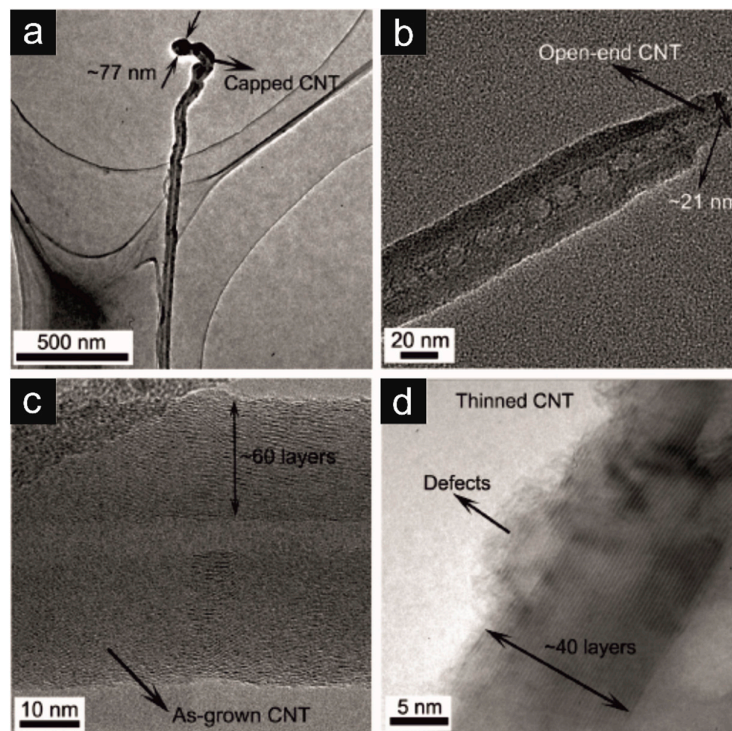


Figure 2. Low-resolution TEM images of (a) capped CNTs and (b) thinned and open-ended CNTs. HR-TEM images of (c) as-grown CNTs with 60 layers and (d) MW-assisted H_2 plasma-processed CNT with ~40 layers and defected outer shells. Reprinted with the permission from Elsevier, Ref. [99].

An important parameter known to influence electrocatalytic and electrochemical properties is surface chemistry [110–113]. So far, two main strategies have been used for the surface modifications. The first strategy involves the post-synthetic treatment of already formed CNs using various oxidizing or reducing agents [114–117]. The second is based on the transformation of the structure by introducing heteroatoms during the formation of CNs, which is called doping [118,119]. For example, doping CNOs with boron (B-CNOs) causes a decrease in the electrical conductivity value due to breaking the outer layer of CNOs [69]. ND-derived CNOs in thermal treatment are spherical structures, mainly with sp^2 -hybridized carbon atoms (Figure 3a). A small addition of pentagons has been identified in systems, like in single-layered fullerenes, which provide structure closure and surface curvature. These topological variations are sp^3 -hybridized and are called defects in sp^2 -hybridized CNs. In Figure 3, some defects are marked with white arrows for visibility. The results obtained by our group showed that the direct doping of CNO with B and N causes the graphitization of the structure and polygonization (Figure 3b). CNOs are in a compressed state, and the spacing between the CNO layers ranges from 0.32 nm to 0.27 nm compared with undoped CNOs (0.34 nm) [34]. The observed structural changes in CNs result in improved electrochemical and electrocatalytic properties of CNs due to numerous defects affecting the increase in porosity and, consequently, the specific surface [34,120].

In many cases, the methods of obtaining CNs at very high temperatures make it impossible to use organic reagents; therefore, to optimize the physical properties of CNs, it is necessary to use post-synthetic treatment. One of the simplest and most frequently used methods leading to numerous structure defects is the chemical oxidation of CNs using various oxidizing reagents [72,121–124]. There are several methods in the literature

where oxidation with a mixture of acids predominates, e.g., HNO_3 or a combination of HNO_3 and H_2SO_4 [72,121], KMnO_4 [122], HCl [123], H_2O_2 [124], or ozone [73]. Chemical treatment leads to the structural degradation of CNs, introducing numerous defects of various sizes, even those that lead to a complete break in the continuity of subsequent layers. In Figure 3d–f, high-resolution TEM images show CNOs subjected to chemical treatment using different oxidative agents. MW irradiation (300 W) was used to obtain CN surfaces with various defects for several minutes. The oxidation of CN surfaces may also be achieved by multiple methods, such as wet chemical oxidation [72], constant potential electrolysis [125], sonochemical or plasma treatment [123,126], etc. In parallel, C atoms are oxidized, forming functional groups containing oxygen, such as aldehydes, ketones, epoxides, esters, alcohols, and carboxylic acids [70,73]. Many works postulate that the presence of oxygen in CNs inhibits the electrocatalytic activity of nanostructures [127,128]. In contrast, oxygen-containing functionalities enhanced the electrochemical properties of CNs [70,129,130]. Additionally, numerous structure defects in the form of holes increase SSA, positively affecting carbon materials' electrochemical properties.

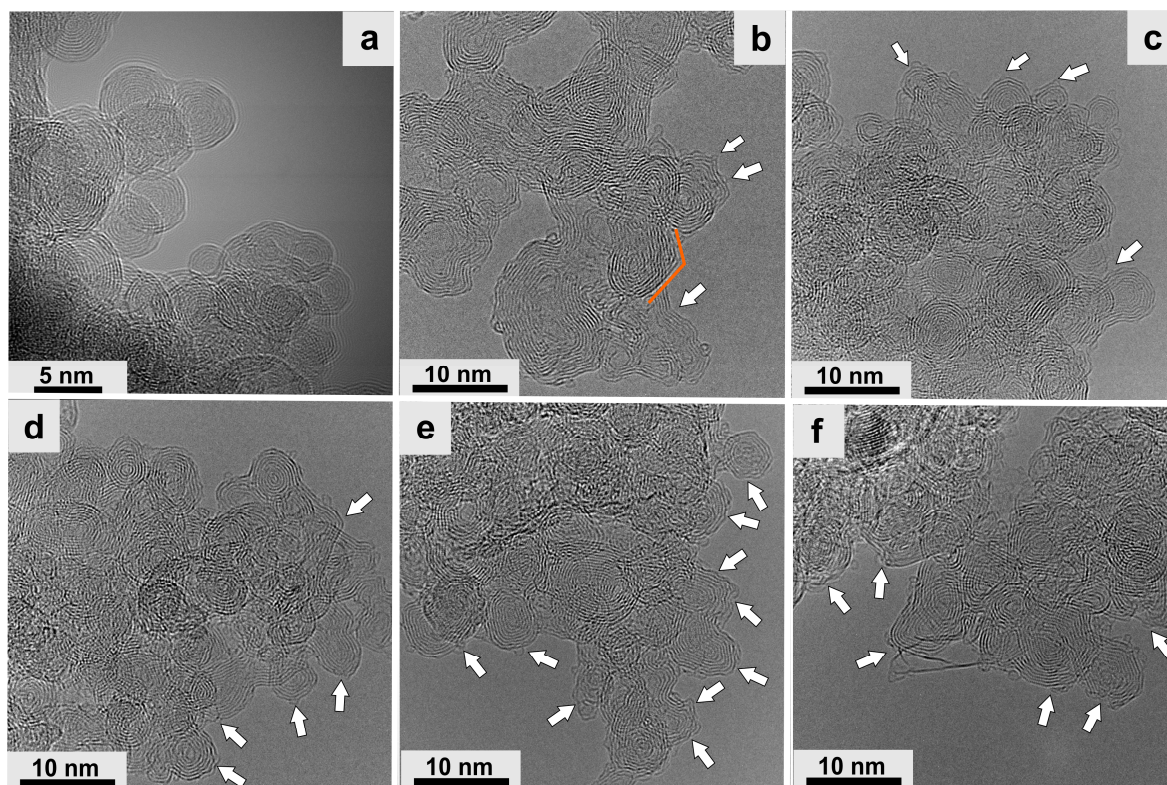


Figure 3. High-resolution TEM images of CNOs obtained from annealing of NDs at 1650 °C in He atmosphere (a) non-modified CNOs, (b) B-doped CNOs, (c) N-doped CNOs obtained from aminated-NDs, (d–f) and modified using MW heating in the presence of different oxidative agents (unpublished results of our group). White arrows indicate different types of structural defects. The orange line highlights the polygonal nature of the CN.

The chemical functionalization of the CN surface also includes a doping that modulates the CN structure [120,131–133], creating defects and, at the same time, increasing the catalytic and electrocatalytic activity [48,117,120,134]. Introducing non-metal dopants into the carbon layer may lead to charge polarization between the heteroatom-doped and the adjacent C atoms due to their different electronegativity [49,135]. Among them, the following stands out (Figure 4) [135]:

- i. N and O acting as electron acceptors or donors for the adjacent C [81,134,136,137];
- ii. B, F, S, and P acting as electron donors for the adjacent C [138–140].

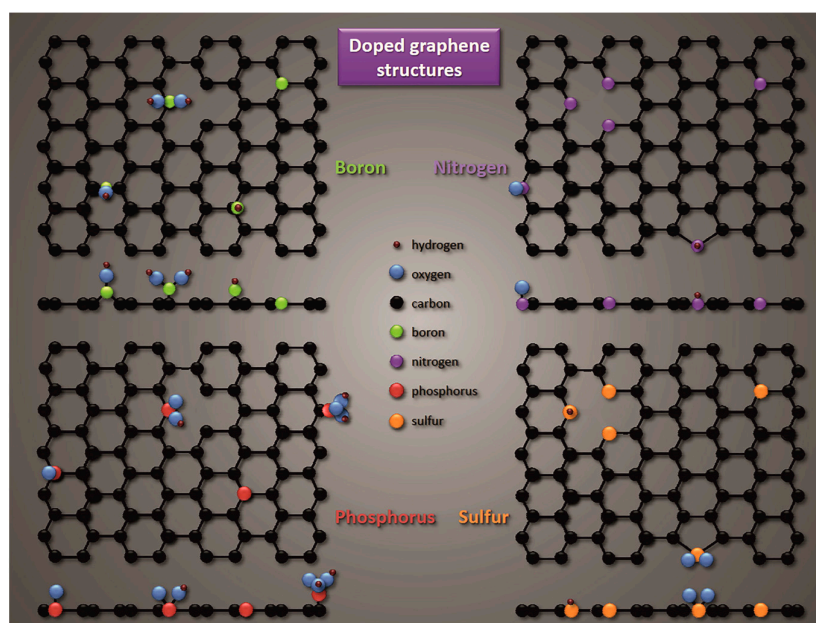


Figure 4. Schematic representation of possible positions for dopant atoms in the graphene network. In each case, the normal and cross-sectional views of the doped material are provided for easier visualization. The representation does not include the actual number of chemical bonds between the elements. Reprinted with the permission from Elsevier, Ref. [135].

Some examples of heteroatom doping are presented in Table 1. The heteroatom incorporation could trigger electron transfer to enhance the electrical conductivity of CNs. On the other hand, the electrical conductivity is determined by the carrier concentration, specific band structure near the Fermi level, and charge distribution. As mentioned earlier, incorporating heteroatoms into the CN creates defects in the structure by changing the local charge and consequently affects the electrical conductivity of the entire nanostructure [55]. The decisive parameters are the charge concentration and distribution (the nature and amount of doped heteroatoms) and the specific structure of the band near the Fermi level [113]. In CNs, localized states appear in the electronic band structure, transforming the passive graphitic network into CNs enriched with reactive sites that interact more strongly with molecules from the external environment [141].

Doping is a critical process that significantly affects the conductive properties of carbon materials, creating electron holes (p-type doping) in the graphene layer or places with an excess negative charge (n-type doping) [118]. Because of the π -conjugation, sp^2 -hybridized CNs can be electron donors or acceptors when coupled with other elements with different electronegativity. Breaking the integrity of the π -conjugation leads to the release of carbon π electrons [37,138,140,142,143]. In N-doped CNs, coupling the C atoms with the lone pair of electrons of the N atoms occurs; as a result, the C atoms adjacent to the N become active [37,144]. Based on measurements made using X-ray photoelectron spectroscopy (XPS), three main groups of N dopants were distinguished (Figure 4):

1. Pyridinic-like N is an atom that combines with two C atoms, enriching the aromatic ring with one p electron (p-type).
2. Pyrrolic-like N is an atom that bonds to two C atoms, sharing two p electrons with the π system (n-type).
3. Graphitic-like N (quaternary) in the graphene layer (in the six-membered ring) is substituted for one C atom (n-type).

We can determine the electronic properties of CNs using, for example, XPS or Near-Edge X-ray Absorption Fine Structure (NEXAFS) C-edge methods (Figure 5) [66]. XPS measurements should be performed for a skinny graphene film, which allows for the determination of changes in the energy states of the CN after its doping with heteroatoms

(Figure 5a). The spectrum of the undoped graphene layer is analogous to that recorded for sp^2 -hybridized carbons [145]. The dominant peak in the spectrum of undoped graphene corresponds to the occupied σ states, and the π states of graphene form the peak at approximately 3.0 eV. The inset in Figure 5a compares spectra, ranging from -2.5 eV to 2.5 eV, normalized to the maximum intensity. In the range of positive values, undoped graphene and P-doped graphene have a similar density of occupied states, while doping with N atoms does not cause a significant increase in the electron density value in the valence band [146]. Unoccupied carbon states in graphene layers were investigated using the NEXAFS C-edge method (Figure 5b). The spectra of undoped graphene and N- or P-doped graphene illustrate electron transitions from the C 1s levels to the partially occupied and empty π and σ states [147]. These transitions use the π^* resonance at 285.4 eV and the σ^* resonance at 291.7 and 292.8 eV [147]. In the graphene spectrum, an apparent splitting of the σ^* resonance into σ_1^* and σ_2^* is visible, indicating the high crystallinity of graphene layers [148]. A band smoothing in the σ^* range is observed for N-doped graphene, indicating numerous defects in the N-doped CNs [149]. The inset in Figure 5b compares the low-energy region of the K-edge C spectra, where the density of unoccupied states increases in the series undoped graphene > P-doped graphene > N-doped graphene. It means that N-doped graphene has the most vacancies and edge defects. Therefore, the low conductivity of graphene layers doped with heteroatoms results from the scattering of charge carriers by heteroatoms and topological defects at the domain boundaries [150].

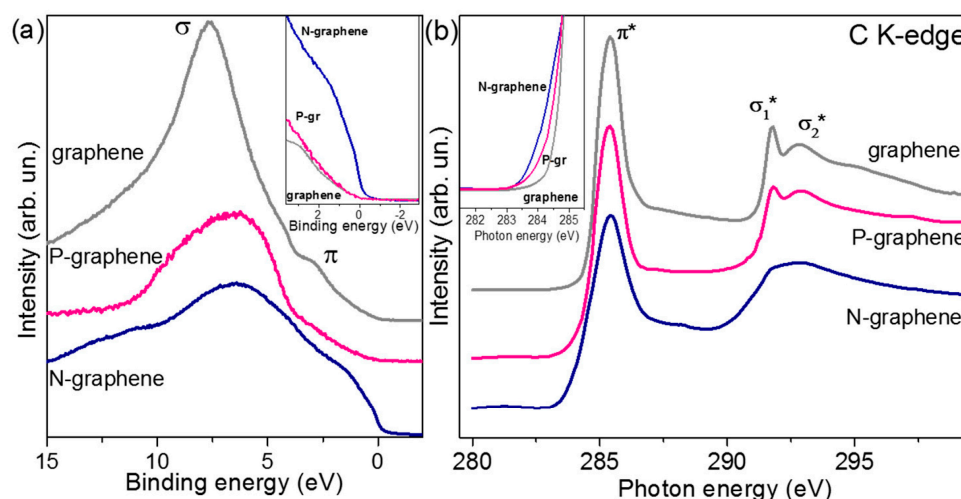


Figure 5. (a) Valence band XPS and (b) near-edge X-ray absorption fine structure (NEXAFS) C K-edge spectra of the annealed graphene, N-graphene, and P-graphene films. Insets show the spectra near the Fermi level. Reprinted with the permission from MDPI, Ref. [66].

Additionally, heteroatom doping, which creates the pyridinic- and pyrrolic-like N atoms, frequently incorporates holes (topological defects) in the graphene layer (Figure 4), which may affect the optimization of the electrochemical properties of the nanostructure by facilitating electrolyte penetration and ion transport. It should also be noted that introducing the N atom into the graphene sheets causes a shift in the conduction band, allowing additional electrons to be adopted. A comparison of the electronic structures of N-doped graphene indicates that graphene with pyridinic-like N systems has the strongest electron deficiency for electron-accepting [81]. Therefore, the pyridinic-like defects are suitable as anode for Li batteries. It has also been shown that quaternary-like defects are suited for Li-ion batteries and offer a lower diffusion and desorption barrier than undoped graphene [139].

The pyridinic-like defects exhibit the nature of Lewis bases, which make them oxygen reduction reaction (ORR) active sites that catalyze O_2 dissociation reactions (Figure 6 and Table 1) [151]. Additional topological defects can enhance the catalytic activity of pyridinic-

like defects. It was demonstrated that monovacancy-coupled pyridinic N sites tuned the electronic properties of C-N bonds. Using the density functional theory (DFT), an energy difference was demonstrated between pyridinic N sites and monovacancy-coupled pyridinic N sites, 398.4 eV and 397.7 eV, respectively. This is related to the different charge distribution within the defects, -0.253 e (pyridinic N sites) and -0.225 e (monovacancy-coupled pyridinic N sites). It, in turn, causes stronger adsorption of oxygen-containing intermediates on the N-doped hierarchical porous carbon (N-HPC) surface and affects the ORR kinetics (Figure 6a–d). The kinetic current density (i_k) for ORR is 19.11 mA/cm² at 0.8 V in an alkaline solution (0.1 M KOH), which is higher than for Pt/C (18.06 mA/cm²) in the same experimental conditions. The N-HPC materials in alkaline solution exhibit an intrinsic turnover frequency of 7.26 times higher than typical pyridinic N atoms, and this is one of the highest values appearing in the literature for metal-free N-doped carbon catalysts. Zn-air batteries using N-HPC as the electrode material have a higher power density of approximately 40% compared with commercial Pt/C catalysts. Increased efficiency in electrocatalysis is also enhanced by the high S_{BET} of 3151.2 m²/g resulting from the enormous micro-mesoporosity of N-HPC.

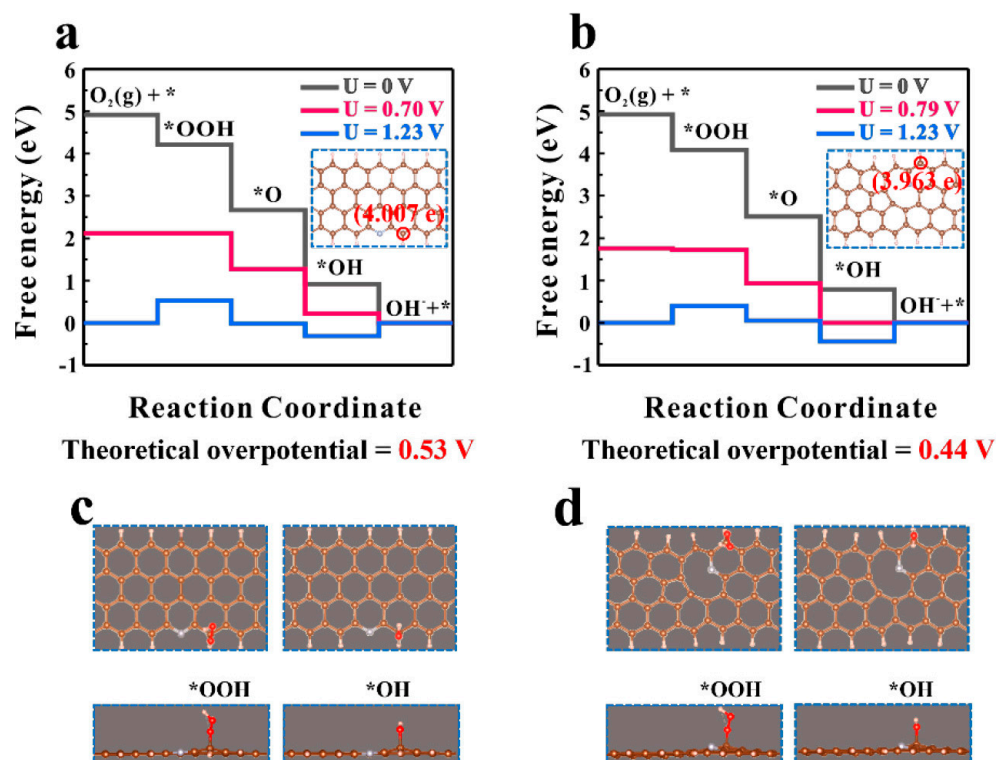


Figure 6. (a) Charge ORR free energy diagrams of (a) conventional pyridinic N site and (b) N-HPC site, optimized adsorption configuration of ORR intermediated (*OOH and *OH) on (c) conventional pyridinic N and (d) N-HPC site (brown, silver, red, and incarnadine balls represent the C, N, O, H atoms, respectively). Reprinted with the permission from American Chemical Society, Ref. [151].

The carbon π electrons in B-doped CNs are activated by conjugating with the vacant $2p_z$ orbital of B, activating the B atoms towards electrocatalysis [36]. The B-doped CNOs exhibited higher tolerances for methanol, higher activities, higher stabilities, and lower costs than commercially used Pt/C. They can be a promising candidate for cost-effective ORR [152–154]. The authors observed the synergistic effect of two kinds of heteroatom-doping (B- and N-co-doped and P- and N-co-doped CNs), where the electron transfer and reaction energy in ORR and oxygen evolution reaction (OER) were strongly affected by the presence of two types of heteroatoms.

Table 1. Some examples of CNs doped by heteroatoms and their short characteristic.

Heteroatom Doping	Substrates	Methods	Carbon Nanostructures	Concentration of Doping Elements	Nature of the Bonding Environment	Significant Properties	Applications	Ref.
Nitrogen	Collagen	Thermal treatment Acid treatment	N-OLC	7.5 at. % N	Pyridinic N Pyrrolic N	Excellent operation stability	ORR catalysis Fuel cells	[114]
	Acetonitrile	Pyrolysis	N-CNO	4.0 at. % N	Pyridinic N Pyrrolic N Graphitic N	Long-term stability	ORR catalysis Nitride sensor	[155]
	Graphene Acetonitrile	CVD	N-Graphene	4.0 at. % N	Pyrrolic N SW defects	High concentrations of defects	Supercapacitor	[55]
	Graphene Melamine	Thermal treatment	N-Graphene	3.7 at. % N	Pyridinic N Pyrrolic N Graphitic N	High current and power density	ORR, OER, HER catalysis	[156]
	Melamine L-cysteine	Polymerization Pyrolysis	N-Graphene nanoribbons	20 at. % N (800 °C) 5.9 at. % N (1000 °C)	Pyridinic N Graphitic N	Bifunctional electrocatalytic activity Excellent cycling stability	ORR and OER catalysis Zn-air batteries	[81]
	GO oxidant	Post-modification	N,O-GON	3.4 at. % N	Pyrrolic N Pyridinic N	High corrosion resistance High selectivity H ₂ O ₂	ORR catalysis	[137]
	CNT Ionic liquid	Carbonization Post-modification	CNT/porous carbon (Core-sheath)	4.6 at. % N 1.1 at. % S 5.4 at. % O	Pyridinic N Pyrrolic N Graphitic N	Durability and tolerance towards methanol	ORR catalysis	[157]
	Aminated-ND particles	Thermal treatment	N-CNO	1.0 at. % N	Pyridinic N Pyrrolic N Graphitic N	Homogenous distributions of defects and active N sites	Electrocatalysis Catalytic activity towards H ₂ O ₂	[48,134]
	SiO ₂ , DCD, APTES, ZIF-8, Zn(NO ₃)·6H ₂ O	Inorganic synthesis Thermal treatment Etching SiO ₂	N-HPC	1.2 at. % N	Monovacancy coupled pyridinic N Graphitic N	Hierarchical porosity S _{BET} = 3151.1 m ² /g	ORR catalysis Zn-air batteries	[151]

Table 1. Cont.

Heteroatom Doping	Substrates	Methods	Carbon Nanostructures	Concentration of Doping Elements	Nature of the Bonding Environment	Significant Properties	Applications	Ref.
Boron	ND particles Amorphous boron	Thermal treatment	B-CNO	0.76–3.21 at. % B	Substitutional B (B-C) Planar BC ₃ nanodomain	High crystallinity Excellent long-term charge/discharge stability	Catalysis Electrochemical capacitors	[34,120]
	ND particles Boric acid	Thermal treatment	B-CNO CNO	0.82–3.31 wt. % B	Boron atom cluster B ₄ C Substitutional B (B-C)	$\sigma = 1.62 \text{ 1}/\Omega\text{cm}$ $\sigma = 0.80 \text{ 1}/\Omega\text{cm}$	ORR catalysis	[69]
	GO, Boric acid	Ultrasonic treatment Hydrothermal reaction	B-rGO	16.2 at. % B	Substitutional B (B-C) BCO ₂ ; BC ₂ O	The lowest onset potential for B-doped graphene (0.83 V vs. RHE)	ORR catalysis	[158]
Multi-heteroatoms	CNT, IL, silica	Post-modification Thermal treatment	N,S,F-CNT	Total N,S,F 8.8 wt. %	Pyridinic N Pyrrolic N Graphitic N	High durability Superior tolerance towards poisons $\sigma(T)/\sigma(T_r) = 163 \text{ S/cm}$ $\sigma(T)/\sigma(T_r) = 184 \text{ S/cm}$	ORR catalysis Alkaline fuel cells	[157]
	Solid graphite rod N ₂ atmosphere Amorphous boron	Arc-discharge evaporation	CNT N,B-CNT	- 0.5 at. % N 0.5 at. % B 1 at. % B and 1 at. % N	Graphitic N N on edges and in topological defects Point substitutional defects C-B and C-N	Charge carriers: $3 \times 10^{18} \text{ cm}^{-3}$ $\sigma(T)/\sigma(T_r) = 314 \text{ S/cm}$ $\sigma(T)/\sigma(T_r) = 493 \text{ S/cm}$	Conductors Magnetoelectronics	[159]
	Melamine Phosphoric acid	Thermal treatment	g-P-C ₃ N ₄	2.69–5.0 at. % N 0.40–3.34 at. % P	C defect coupled with N doping Substitutional B (B-C) BC ₃ ; BCO ₂ ; BC ₂ O	High graphitization Edge defects	ORR catalysis	[160]
	ND Boric acid	Thermal treatment	N-B-CNO	8.0 at. % B 7.4 at. % N	Pyridinic N Pyrrolic N Graphitic N; B-N	High degree of defects	ORR catalysis	[161]

Abbreviations in alphabetical order. APTES: (3-aminopropyl)triethoxysilan; CNC: carbon nanocages; CNO: carbon nano-onion; CNT: carbon nanotube; CVD: chemical vapour deposition; DCD: dicyandiamide, g-C₃N₄: graphitic carbon nitride; GO: graphene oxide; GQD: graphene quantum dot; GON: graphene oxide nanoribbons; HER: hydrogen evolution reaction; N-HPC: nitrogen-doped hierarchical porous carbon; IL: ionic liquid; ND: nanodiamond; OER: oxygen evolution reaction; OLC: onion-like carbon; ORR: oxygen reduction reaction; rGO: reduced graphene oxide; ZIF-8: zeolitic imidazolate framework compound. σ : electrical conductivity; $\sigma(T)/\sigma(T_r)$: conductivity normalized to room temperature; S_{BET} : specific surface area determined using BET theory.

Only such atomic configurations of the B and N–pyridinic active sites were preferred, with a small distance between the two atoms. The DFT calculations showed that the chemical coupling of the B and N–pyridinic active sites occurred then, increasing ORR activity. In acidic electrolytes, CNs co-doped with N and S are very promising [36]. The N–C–S–defect-based motifs in carbon materials decreased the energy barriers for ORR in acidic solutions, making the material better than the Pt/C commercial electrocatalyst.

All these factors may consequently lead to an enhancement of the catalytic efficiency due to the increasing of active sites in CNs [81,162–164]. The latter results from the doping process using various substrates and methods. We can distinguish thermal treatment at the gaseous atmosphere and reduced pressure [114,136,157], pyrolysis [136], CVD [55], MW-assisted synthesis [165], arc-discharge evaporation [159], etc., (Table 1). Some of these methods are used as one-step processes; others must be supported by multi-step strategies that optimize the reaction conditions. The catalytic activity of CNs is also affected by their morphology, mainly the type of surface determined by their porosity [49]. The size of the pores (micro-, meso- and macropores), their number, and their arrangement affect the efficiency of the catalytic reaction:

- i. micropores allow more active sites into the electrolyte;
- ii. mesopores can facilitate the mass transport in the catalyst layer;
- iii. macropores ensure the catalyst's long-term stability [49].

Zheng Hu and coworkers presented an example of carbon nanocage preparation and the influence of d-CNs on electrocatalytic activity in 2015 [37]. Carbon nanocages were synthesized by the hard-templating method from benzene as the precursor. Next, the pyrolysis results in forming carbon nanocages with a cuboidal hollow structure 10–20 nm in size. This size corresponds to the thickness of the coating from four to seven graphitic layers (Figure 7a). Increasing the temperature from 700 to 900 °C led to an increase in the nanocages' average size and wall thickness. Temperature also affects the distribution of pores and the number of defects in the structure. Micropores (~0.6 nm) and mesopores (5–50 nm) coexist in the materials. However, an increase in temperature causes the pore distribution to shift toward the mesopores (Figure 7b) while reducing the SSA from 1713 m²/g (700 °C) to 614 m²/g (900 °C). As the temperature increases, the crystallinity of the material increases, i.e., the number of defects in the material decreases (Figure 7c). The highest concentration of the defects was detected for the material pyrolyzed at 700 °C. The observed defects in the carbon nanocages are topological disclinations (Figure 7d), in which zigzag edge and pentagon defects are responsible for the electrocatalytic activity of these CNs.

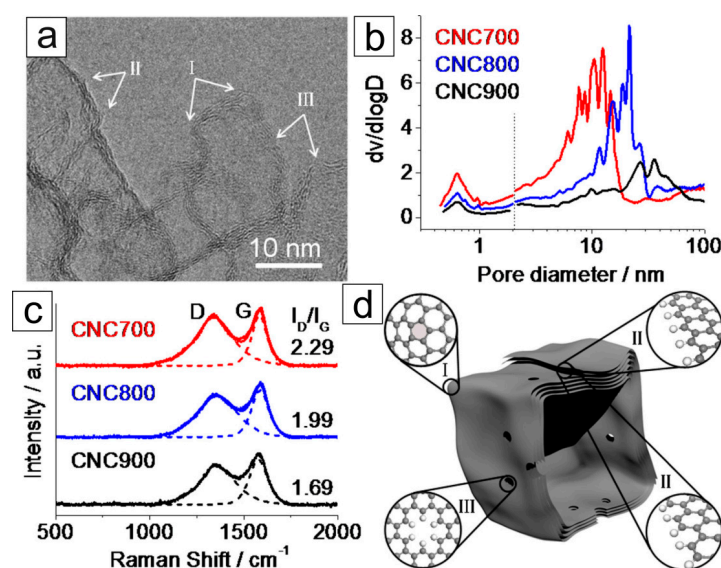


Figure 7. Characterizations and schematic structural characters of the carbon nanocages. (a) High-resolution TEM image of CNC700. (b) Pore size distributions. (c) Raman spectra. I_D/I_G is the area

ratio of the D peak to the G peak. (d) Schematic structural characters of the carbon nanocages. I, II, and III in panels (a,d) represent three typical defective locations, i.e., the corner, the broken fringe, and the hole, respectively. Reprinted with the permission from American Chemical Society, Ref. [37].

4. MW-Assisted Synthesis for the Preparation and Modification of Materials Containing d-CNs

4.1. Definition of MW-Assisted Synthesis

MW irradiation is an influential heating parameter for carbon-based solid materials because they usually absorb electromagnetic radiation well [166,167]. This high-frequency electromagnetic radiation with a wavelength between 0.001 and 1 m (frequencies between 300 and 0.3 GHz) can achieve a temperature of over 1000 °C within a few minutes. Heating of the material is possible due to the interaction of electromagnetic radiation of appropriate energy with charged particles (Figure 8) [168,169]. When polar molecules interact with MW radiation, this causes them to rotate and move, and this, in turn, causes friction. Consequently, the generated energy is dissipated as heat (dipolar polarization). In the case of solid phase materials that are dielectrics, charged particles such as π electrons in carbon materials induce a current flow in the material. In this case, the energy is also dissipated as heat, related to the Maxwell–Wagner effect (interfacial polarization). For the optimal interaction of MW with solid materials, its penetration depth must also be considered [168]. However, it has to be noted that penetration depth becomes a critical factor in micron-scale materials. For the materials in the nanoscale, this problem should not occur.

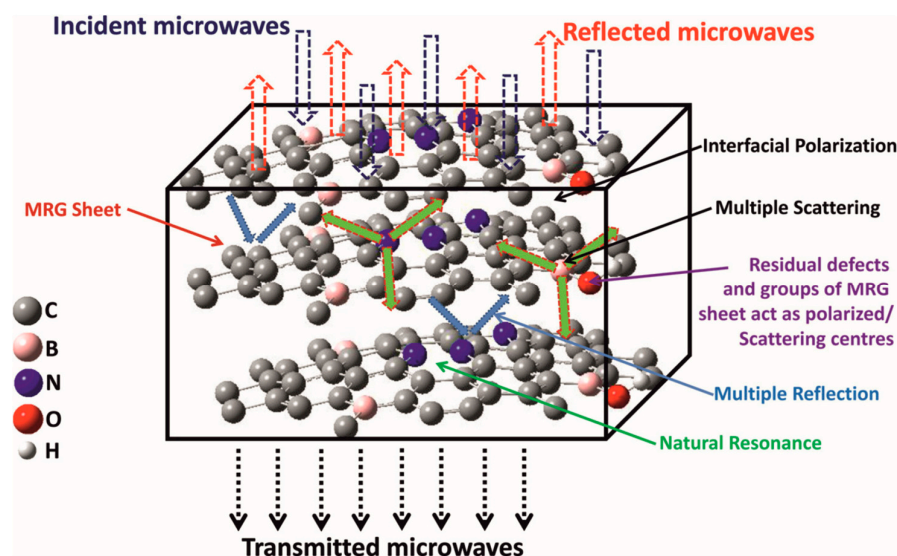


Figure 8. Schematic representation of possible MW absorption mechanism in B- and N-doped porous graphene sample. Reprinted with the permission from American Chemical Society, Ref. [170].

Significant advantages of using MW heating [167]:

- i. contactless heating;
- ii. a direct transfer of energy to the reactants;
- iii. independence from heat convection;
- iv. rapid heating rates, easy control of irradiation parameters;
- v. selectivity of heating;
- vi. the possibility of conducting the reaction locally and volumetrically.

The MW-based methods may be divided into two groups:

1. Top-down methods, which include the transformation of solid materials into carbon nanomaterials.
2. Bottom-up methods, which include the preparation of carbon nanomaterials from liquid or gaseous carbonaceous precursors.

It is possible to use the energy of the MW irradiation to create new carbon materials and as a method for the purification, functionalization, or annealing of CNs [169]. It is often a method supporting other processes and procedures. Depending on the specific structural properties of the CNs, MW irradiation interacts specifically with the material due to the particular absorption properties of the CNs [171]. The temperature reached in a given process will depend on many parameters. Depending on the type of CNs, their purity (for example, metallic dopants), the defects' structure, creates functional groups on the surface (for example, containing oxygen), and during the interaction of the carbon material with MW irradiation, local heating may occur. Conversely, when the carbonaceous material is a poor absorber of MW irradiation, it is necessary to add substances to make the MW heating process more efficient [168,172]. In this case, substances such as polymers, conducting materials or ionic materials, metallic nanoparticles, etc., should be applied [173–175].

4.2. MW-Assisted Synthesis for the Preparation and Modification of d-CNs: Implications on Properties and Applications

MW-assisted synthesis is a powerful heating method for preparing or modifying carbon-based solid materials [176]. Currently, this method is most often used to design and modify graphene (G), carbon nanotubes (CNTs), carbon quantum dots (CQDs), and graphitic nitride carbon ($g\text{-C}_3\text{N}_4$). By MW-assisted heating with the different carbon sources (graphite [177,178], metallocenes [171,178], carbon nanoparticles [179], polymers [180,181], etc.) in the presence of a catalyst and in the gas phase, different CNs were synthesized (Table 2).

Non-modified CNs have somewhat limited charge accumulation properties [182–184]. To optimize the electrochemical properties of carbon materials, they are combined with redox capacitive materials, which are involved in faradaic reactions. Combining the mechanical and electrochemical stability of CNs and their high SSA resulting from micro-mesoporosity produces hybrid materials with excellent electrochemical properties. Examples of the hybrid materials synthesized using MW irradiation are listed in Table 2, and their specific parameters determine subsequent applications. The optimized electrochemical properties of the mixed materials are mainly due to the possibility of creating mesoporous inorganic structures with different structural characteristics (amorphous and crystalline materials) combined with highly conductive CNs. Depending on the experimental conditions of the MW synthesis, it is possible to create materials with a different degree of structure organization with a higher degree of crystallinity, leading to obtaining composites with better electrochemical properties. For example, an rGO/Fe₃O₄ composite was obtained in which the Fe₃O₄ inorganic phase was in the form of nanoparticles or octahedral nanocrystals (Table 2) [185]. In this case, the organization of Fe₃O₄ into octahedral crystals on the rGO surface increased the C value from 1050 to 1625 mA h/g at a current density (*j*) of 100 mA/g.

Table 2. Some examples of using MW-assisted synthesis for the preparation and modification of pristine d-CNs and hybrid materials containing d-CNs.

Defective CNs	Materials Containing d-CNs	Methods	Experimental Conditions	Applications	Significant Properties	Refs.
Pristine d-CNs	d-G (hydrogel)	MW-assisted hydrothermal synthesis	$P = 800 \text{ W}; t = 5 \text{ min}$	Supercapacitors	$C_s = 340 \text{ F/g}$ ($j = 0.5 \text{ A/g}$)	[186]
	N,S-GO	MW-assisted synthesis	$P = 800 \text{ W}; t = 5 \text{ min}$	Supercapacitors Universal: aqueous, non-aqueous, ionic electrolytes	$C_s = 460 \text{ F/g}$ ($j = 1 \text{ A/g}$) $C_s = 810 \text{ F/g}$ ($j = 3 \text{ A/g}$)	[118]
	S-rGO	MW-assisted synthesis	$T = 140 \text{ }^\circ\text{C}; t = 30 \text{ min}$	Supercapacitors	$C_s = 238 \text{ F/g}$	[187]
	rGO	Chemical synthesis	$P = 700 \text{ W}; t = 40 \text{ s}$	EMI shielding devices	$\sigma = 21.4 \text{ S/m}$	[170]
	N,B-rGO	MW-assisted synthesis	$P = 700 \text{ W}; T = 180 \text{ }^\circ\text{C}; t = 6 \text{ min}$	Supercapacitors	$\sigma = 124.4 \text{ S/m}$	[188]
	rGO (porous)	MW-assisted synthesis	$P = 700 \text{ W}; T = 180 \text{ }^\circ\text{C}; t = 6 \text{ min}$	Supercapacitors	$C_s = 568 \text{ F/g}$ ($j = 1 \text{ A/g}$)	[188]
	rGO	IL-assisted MW synthesis	$P = 700 \text{ W}; t = 15 \text{ s}$	Supercapacitors	$C_s = 135 \text{ F/g}; E_m = 58 \text{ Wh/kg}; P_m = 246 \text{ kW/kg}$	[189]
	d-CNT	MW hydrogen plasma processing	$P = 200 \text{ W}; t = 30 \text{ and } 60 \text{ min}$	Vacuum electron sources	$j_{\text{emission}} = 10.36 \text{ mA/cm}^2$	[106]
	GO/g-C ₃ N ₄	Ultrasonic-MW-assisted synthesis	$P = 700 \text{ W}; t = 5 \text{ min}$	Photocatalytic H ₂ evolution	Photocatalytic H ₂ -production rate 224.6 $\mu\text{m}^3/\text{h}$; GO electron collector and transporter	[190]
	GO/g-C ₃ N ₄	MW-assisted synthesis Chemical treatment	$P = 700 \text{ W}; t = 5 \text{ min}$	Supercapacitors	$S_{\text{BET}} = 353 \text{ m}^2/\text{g}; C_s = 113 \text{ F/g}$ $S_{\text{BET}} = 686 \text{ m}^2/\text{g}; C_s = 169 \text{ F/g}$	[191]
N-PGF	MW-assisted synthesis	$P = 800 \text{ W}; t = 4 \text{ s}$	Supercapacitors	$C_s = 272.6 \text{ F/g}; E = 2.3 \text{ mW h/cm}^2; P = 0.42 \text{ W/cm}$	[192]	
Hybrid materials containing d-CNs	CNT/Fe ₂ O ₃	CVD; MW hydrothermal synthesis	$T = 160 \text{ }^\circ\text{C}; t = 6 \text{ h}$	Lithium-Ion Battery Electrodes	$C = 900 \text{ mAh/g}$	[193]
	CNT/NiMn ₂ O ₄	MW-assisted hydrothermal synthesis	$P = 800 \text{ W}; T = 160 \text{ }^\circ\text{C}; t = 1 \text{ h}$	Supercapacitors	$C_s = 916 \text{ F/g}$ ($j = 1 \text{ A/g}$) $E_m = 36.5 \text{ Wh/kg}; P_m = 800 \text{ W/kg}$	[194]
	MWCNT/CoMoO ₄	MW-assisted solid-state synthesis	$P = 480\text{--}720 \text{ W}; t = 8 \text{ min}$	Supercapacitors	$C_s = 170 \text{ F/g}$ ($j = 0.1 \text{ A/g}$)	[195]
	NiS@CNT/NiO	MW-assisted solid-state synthesis	$P = 1000 \text{ W}; t = 60 \text{ s}$	Supercapacitors	$C_s = 810 \text{ F/g}$ ($j = 1 \text{ A/g}$)	[196]

Table 2. Cont.

Defective CNs	Materials Containing d-CNs	Methods	Experimental Conditions	Applications	Significant Properties	Refs.
Hybrid materials containing d-CNs	rGO/NiS	MW-assisted hydrothermal synthesis	$P = 700 \text{ W}; t = 4 \text{ min}$	Supercapacitors Solid-state	$C_s = 1746 \text{ F/g}$ ($j = 1 \text{ A/g}$) $C_s = 14.20 \text{ F/g}$;	[197]
	rGO/Fe ₃ O ₄ NPs	Chemical exfoliation	$P = 700 \text{ W};$	Supercapacitors	$E_m = 7.1 \text{ Wh/kg}; P_m = 1836 \text{ W/kg}$	[185]
	rGO/Fe ₃ O ₄ ONCs	MW-assisted synthesis	$t = 1.25\text{--}1.75 \text{ min}$	Lithium-Ion Battery Electrodes	$C = 1050 \text{ mA h/g}$ ($j = 100 \text{ mA/g}$) $C = 1625 \text{ mA h/g}$ ($j = 100 \text{ mA/g}$)	
	rGO/CNT/Ni _{NP}	Thermal exfoliation	$P = 700 \text{ W}; t = 5 \text{ min}$	Lithium-Ion Battery Electrodes	$C = 648.2 \text{ mA h/g}$ ($j = 100 \text{ mA/g}$) $C = 282.4 \text{ mA h/g}$ ($j = 100 \text{ mA/g}$)	[198]
	rGO/NiO/Co ₃ O ₄	MW-assisted synthesis	$P = 700 \text{ W}; t = 45 \text{ s}$	Supercapacitors	$C_s = 910 \text{ F/g}$ ($v = 20 \text{ mV/s}$) $S_{BET} = 99.5 \text{ m}^2/\text{g}$	[199]
	rGO/CoAl-LDH	MW-assisted reflux synthesis	$P = 1000 \text{ W}; T = 100 \text{ }^\circ\text{C};$ $t = 2 \text{ h}$	Supercapacitors	$C_s = 772 \text{ F/g}$ ($j = 1 \text{ A/g}$) $E_m = 22.7 \text{ Wh/kg}; P_m = 230 \text{ kW/kg}$	[200]
	rGO/NiAl-LDH	MW-assisted reflux synthesis	$P = 1000 \text{ W}; T = 100 \text{ }^\circ\text{C};$ $t = 2 \text{ h}$	Supercapacitors	$C_s = 1630 \text{ F/g}$ ($j = 1 \text{ A/g}$) $S_{BET} = 121.2 \text{ m}^2/\text{g}$	[201]
	rGO/NiMoO ₄	MW-solvothermal synthesis Thermal annealing	$P = 200 \text{ W}; T = 115 \text{ }^\circ\text{C};$ $t = 25 \text{ min}$	Supercapacitors	$C_s = 1274 \text{ F/g}$ ($j = 1 \text{ A/g}$) $S_{BET} = 50.8 \text{ m}^2/\text{g}$ $C_s = 800 \text{ F/g}$ ($j = 1 \text{ A/g}$) $S_{BET} = 30.9 \text{ m}^2/\text{g}$	[202]
	N-G/NiS	MW-assisted synthesis	$P = 336 \text{ W}; t = 18 \text{ min}$	Supercapacitors	$C_s = 1468 \text{ F/g}$ ($j = 1 \text{ A/g}$) $E_m = 66.6 \text{ Wh/kg}; P_m = 405.8 \text{ W/kg}$	[203]
	rGO/MnCo ₂ O ₄	Exfoliation MW-assisted synthesis	$P = 900 \text{ W}; t = 45\text{--}70 \text{ s}$	Supercapacitors	$C_s = 562 \text{ F/g}$ ($v = 20 \text{ mV/s}$)	[204]
	G/ α -MoO ₃	MW-assisted synthesis	$P = 700 \text{ W}; t = 7 \text{ min}$	Supercapacitors	$C_s = 483 \text{ F/g}$ ($j = 1 \text{ A/g}$)	[205]
	rGO/CoSe ₂	MW-assisted synthesis Thermal annealing	$P = 700 \text{ W}; t = 7 \text{ min}$	Supercapacitors LED	$C_s = 761 \text{ F/g}$ ($j = 1 \text{ A/g}$) $E_m = 43.1 \text{ Wh/kg}$	[206]
	G/Co ₉ S ₈	MW-assisted hydrothermal synthesis	$P = 700 \text{ W}; T = 160 \text{ }^\circ\text{C};$ $t = 30 \text{ min}; p = 8 \times 10^6 \text{ Pa}$	Supercapacitors	$C_s = 1150 \text{ F/g}$ ($v = 5 \text{ mV/s}$)	[67]
	rGO/MnN	MW-assisted synthesis	$P = 900 \text{ W}; t = 1 \text{ min}$	Sodium ion batteries Supercapacitors	$C = 16 \text{ mAh/g}$ $C_s = 639.2 \text{ F/g}$ ($v = 10 \text{ mV/s}$)	[207]

Table 2. Cont.

Defective CNs	Materials Containing d-CNs	Methods	Experimental Conditions	Applications	Significant Properties	Refs.
Hybrid materials containing d-CNs	rGO/MnO ₂	Conventional synthesis MW-assisted synthesis	$P = 700 \text{ W}; t = 2 \text{ min};$ 21 cycles	Supercapacitors	$C_s = 140 \text{ F/g} (j = 1 \text{ A/g})$	[208]
	rGO/Pd	MW-assisted synthesis	$P = 810 \text{ W}; t = 90\text{--}125 \text{ s}$	Electrocatalysis (Ethanol Oxidation)	Catalytic activity 10.2 mA/cm^2 (Pd)	[209]
	S-rGO/NiFeS ₂	MW-assisted synthesis	$P = 800 \text{ W}; t = 3 \text{ min}$	Supercapacitors	$C_s = 1073 \text{ F/g} (j = 1 \text{ A/g})$ $E_m = 45.7 \text{ Wh/kg}; P_m = 222 \text{ W/kg}$	[210]
	3D Pd-E-PG	MW-assisted synthesis	$P = 700 \div 900 \text{ W};$ $t = 30 \div 60 \text{ s}$	H ₂ storage CO oxidation	H ₂ 5.4 wt. % 100% CO conversion < 300 °C	[211]
	NiF-G/SimonK	MW-hydrothermal synthesis	$P = 700 \text{ W}; t = 1 \text{ h};$ $p = 100 \text{ bar}$	Supercapacitors	$C_s = 836 \text{ F/g} (j = 1 \text{ A/g})$	[212]
	G/NiCoS	MW-assisted synthesis	$P = 600 \text{ W}; t = 20 \text{ min}$	Supercapacitors	$C_s = 1186 \text{ F/g} (j = 1 \text{ A/g})$ $E_m = 46.4 \text{ Wh/kg}$	[213]
	G/CNT/Pd	IL-assisted MW synthesis	$P = 700 \text{ W}; t = 10 \text{ min}$	Energy storage systems	$C_s = 1615 \text{ F/g} (v = 10 \text{ mV/s})$	[214]
	CMK-3/CNT	Hard-templating method MW-assisted synthesis	$P = 700 \text{ W}; t = 30 \text{ s}$	Supercapacitors	$C_s = 315 \text{ F/g} (j = 1 \text{ A/g})$	[68]

Abbreviations in alphabetical order. CMK-3: ordered mesoporous carbon; CNT: carbon nanotubes; CQD: carbon quantum dot; d-CNT: defective carbon nanotube; DSSC: dye-sensitized solar cells; EMI: electromagnetic interference; G: graphene; GO: graphene oxide; rGO: reduced graphene oxide; g-C₃N₄: graphitic carbon nitride; LDH: layered double hydroxide; LED: light emitting diode; MnN: manganese nitride; MWCNT: multi-walled carbon nanotube; NP: nanoparticle; N-PGF: nitrogen-doped porous graphene framework; NCS: nickel cobalt sulfides; NiF: nickel foam; ONC: octahedral nanocrystal; ox-CNT: oxidized carbon nanotubes; o-PDA-co-PANI: copolymer of *ortho*-phenylenediamine and aniline; 3D Pd-E-PG: Pd-embedded three dimensional porous graphene; SimonK: Simonkolleite (Zn₅(OH)₈Cl₂·H₂O). Physical quantities: σ : electrical conductivity [S/m]; E_m : specific energy density [Wh/kg]; j : current density [A/g]; p : pressure; P_m : specific power density [W/kg]; P : power [W]; T : temperature [°C]; t : time; S_{BET} : specific surface area determined by N₂ adsorption method using BET theory.

Although for most hybrid systems, the SSA values determined usually have low values below $100 \text{ m}^2/\text{g}$, the synthesized materials show superior capacitive performance (Table 2). Firstly, the addition of CNs to the inorganic phase decreases the degree of aggregation of the inorganic material. The total capacity of the electrode is related to two charging mechanisms: electric double-layer charging (EDLC) and pseudocapacitance [130,215]. The first process is related to the presence of carbonaceous material in the structure, and, to put it simply, the capacitance of the EDLC depends on the SSA [216]. The second mechanism is based on the redox reaction of the inorganic material, mainly transitional metal oxides and multiplex systems with stoichiometric and nonstoichiometric compositions [215]. Since the percentage of inorganic components in the composite is usually several times higher than CNs, this mechanism is dominant in hybrid electrodes [217]. As a result, in composite electrodes, in which there is good contact between the organic and inorganic phases, and their homogeneous dispersion is ensured, the communication between electrolyte ions and active electrochemical materials is facilitated, and the ion diffusion path is shortened. It is essential to point out that the presence of CNs in the composite decreases the material's resistance and increases its cycling stability as well as energy density (E) and power density (P) compared with pristine inorganic materials [217]. Table 2 summarizes examples of d-CNs and hybrid systems obtained using MW irradiation, indicating the materials' reaction parameters and critical properties.

Figure 9 presents two examples of MW irradiation's use for synthesizing different compositions of carbon-based materials. Panel (I) shows the preparation of N-doped carbon quantum dot (N-CQD)/MWCNT material using the conventional method and MW-assisted synthesis [218]. The first stage of the process was based on the most popular method of MWCNT oxidation using concentrated nitric acid. As a result of this reaction, oxygen-containing functional groups were introduced on the MWCNT surface. In the further stage of the reaction, these sites (structural defects) are active for further functionalization. Further, in the presence of urea and citric acids and under heating, N-CQDs are formed on the surface of MWCNTs (Figure 9I). The authors of this work also carried out, for comparison, the stage of N-CQD production under conventional reaction conditions. The data summarized in Table 2 indicate that using MW irradiation to synthesize N-CQDs shortens the reaction time and energy consumption and increases the efficiency of the reaction. Figure 9II shows the possibility of the multifunctional use of MW irradiation, depending on the power and duration of its use (see also Table 2). Kumar and colleagues used the MW irradiation process to obtain nanohole-structured and Pd-embedded 3D porous graphene (3D Pd-E-PG) [211]. The process was multi-stage. The first stage was graphene's exfoliation and the addition of ethanol and Pd acetate to the reaction mixture. Then, under the influence of MW irradiation with a power of 700 W, within 30 s, Pd nanoparticles were created. Next, MW irradiation with a power of 700 W for 60 s was applied again, which caused the formation of a 3D structure consisting mainly of the agglomeration of Pd nanoparticles. In the last stage of the process, a higher power MW irradiation (900 W, 60 s) was used, which caused the perforation of the graphene layer (creation of defects). Holes of a size analogous to Pd nanoparticles enabled the distribution of nanoparticles in the entire volume of the carbon material, creating a compact and interconnected structure of 3D Pd-E-PG. The course of each stage was confirmed using scanning electron microscopic (SEM) imaging (Figure 9II(a–d)). Figure 9II(a) shows the graphene layers, which, resulting from MW irradiation, form a brush-like and wrinkled structure. In the next stage, the Pd nanoparticles are evenly distributed on the graphene layers (Figure 9II(b)). As a result of the MW irradiation of a specific time and power, the graphene layers are covered with a large amount of Pd nanoparticles. Further irradiation leads to the formation of nanoholes (10–100 nm) (Figure 9II(c,d)), in which metallic nanoparticles are placed, creating a 3D structure of Pd-E-PG, with the simultaneous formation of increasingly larger metallic agglomerates.

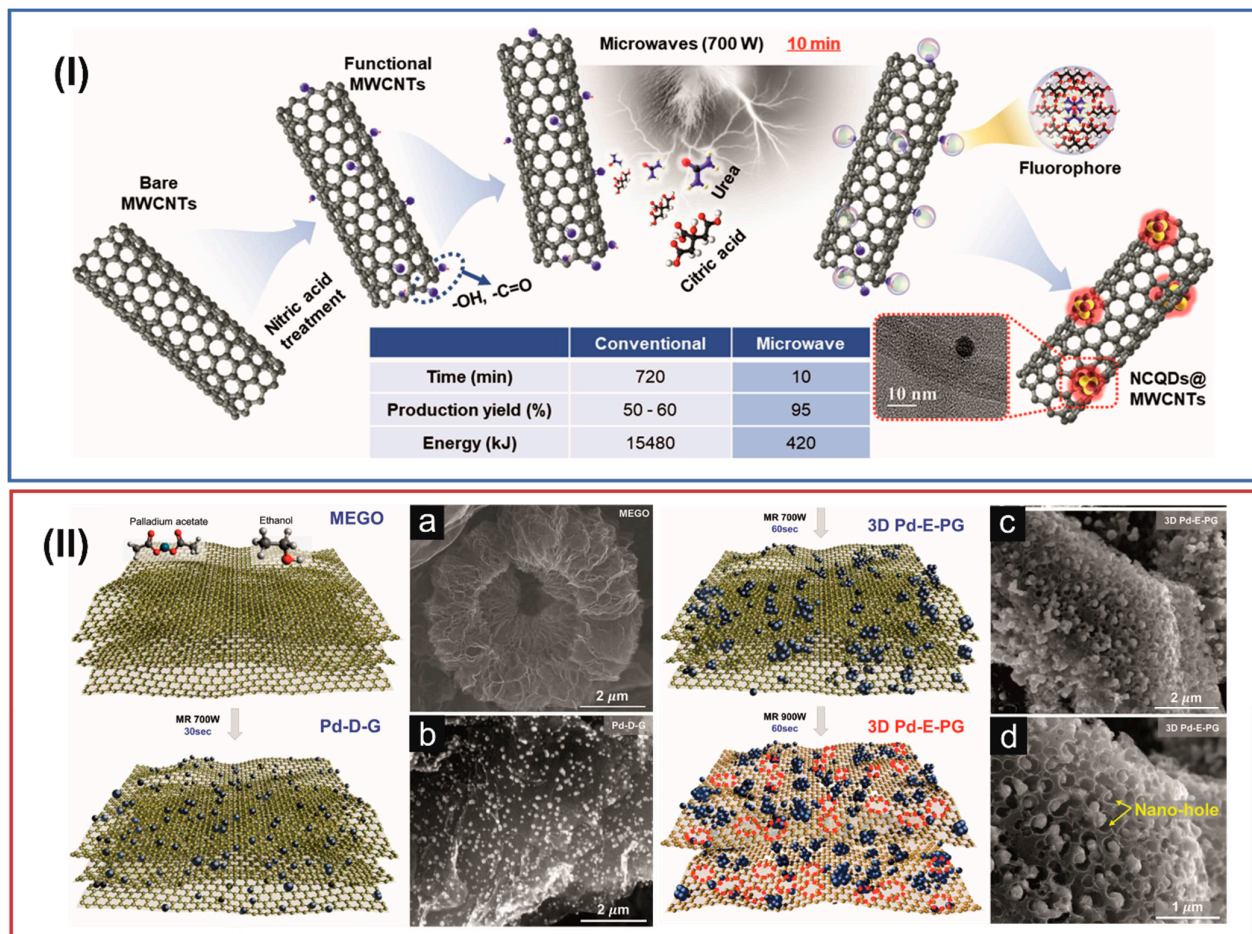


Figure 9. Panel (I): Schematic illustration of the synthesis of MWCNT/N-CQD, where mild oxidation generates active sites for the growth of N-CQDs. The inset table compares the conventional synthesis with the MW-assisted process. Reprinted with the permission from Elsevier, Ref. [218]. Panel (II): Synthesis route of nanohole-structured and Pd-embedded 3D porous graphene (3D Pd-E-PG) and corresponding SEM images. Schematic illustration of the MW fabrication process of the 3D Pd-E-PG. (a) SEM image of MW-exfoliated graphene oxide. (b) SEM image of the uniform decoration of Pd nanoparticles on graphene layers after low-power MW irradiation. (c) SEM image of the aggregation of Pd nanoparticles after successive high-power MW irradiation. (d) SEM image of nanohole generation and the perforated graphene structures after multistep MW irradiation. Reprinted with the permission from American Chemical Society, Ref. [211].

Generally, the synthesis or modification of carbon-based materials using MW irradiation follows the presented paths. In some cases, running the reaction in multiple steps is necessary, mainly to increase the yield of the reaction. Despite this, the procedures are much more straightforward, thanks to the short reaction times under MW-assisted heating. In addition, in the case of these methods, the purification process is much simpler.

Graphene is a 2D atomic crystal with extreme mechanical strength and high electronic and thermal conductivities [219]. Due to these outstanding properties, it has been one of the most frequently used CNs in scientific research in recent years [220]. In the case of this carbon structure, MW irradiation is not used to prepare it in bottom-up processes. However, due to its simplicity, MW irradiation modifies a graphite precursor. Exfoliation is therefore possible, yielding graphene oxide (GO) [221]; the reduction of GO [186], resulting in reduced GO (rGO) [188]; the doping of graphene layers with heteroatoms [118,187,189], or a combination of two kinds of CNs in one material [190,192].

MW irradiation is often used to functionalize graphene layers [222]. The controlled creation of defects in graphene-based materials is a promising strategy to tailor the elec-

trical, electrochemical, and electrocatalytic properties. For example, a hydrogel was obtained from oxidized graphene during MW-assisted synthesis in hydrothermal conditions (Figure 10a) [186]. This one-step process resulted in a 3D carbon structure resembling crinkled paper. Such a 3D graphene structure can accelerate the transport and diffusion of ions, and functional groups reduce the aggregation of graphene layers. The obtained material exhibits a high specific capacitance (C_S) of 340 F/g at j of 0.5 A/g and excellent stability with approximately 97.3% retention of the initial C_S after 20,000 cycles (at 10 A/g) (Table 2). These parameters indicate that d-G (hydrogel) may be a promising electrode material for high-performance SCs.

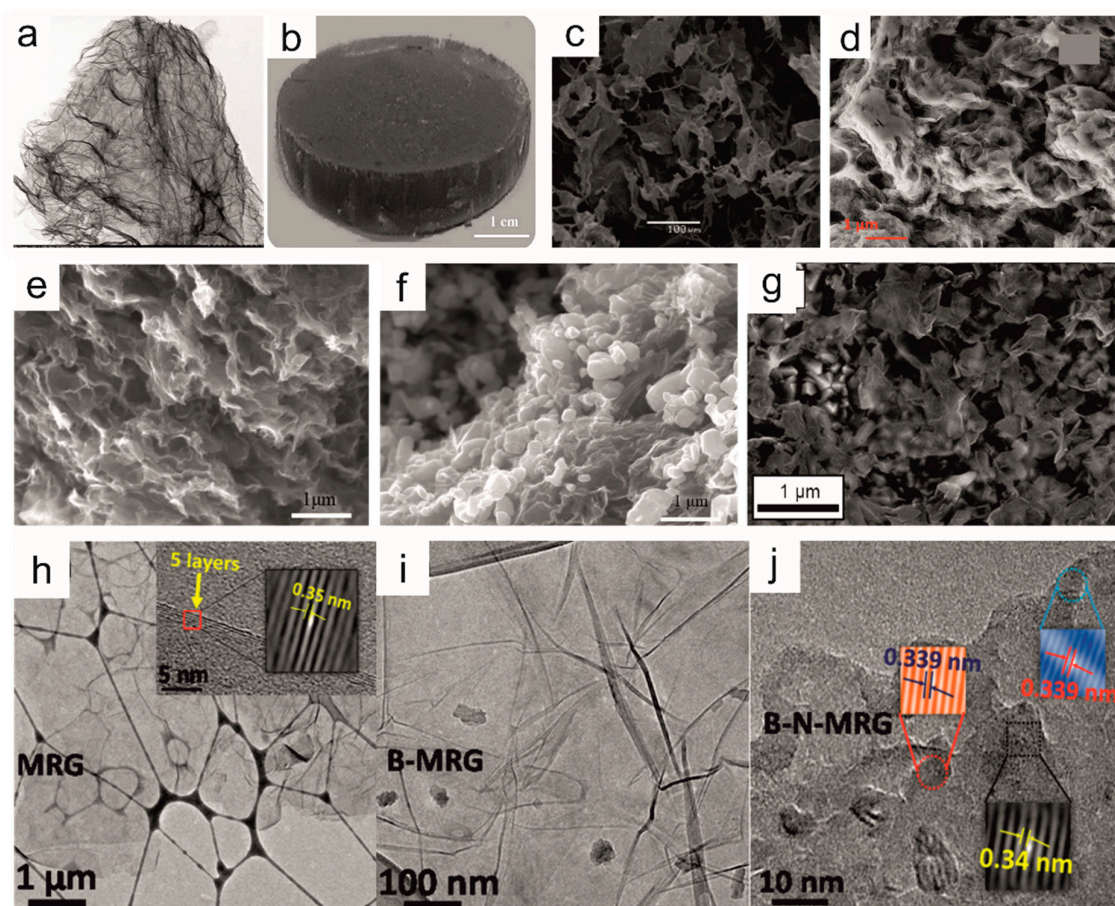


Figure 10. SEM image of (a) functionalized graphene [186]. (b) Photograph of gelatin-GO aerogel [221] and (c) SEM image of gelatin-GO aerogels [221]. SEM images of (d) 1:1.5 nickel-cobalt sulfides [118], (e) porous rGO (GO:ZnO = 1:4) [188], (f) rGO/ZnO (GO:ZnO = 1:4 (without HCl)) composites [188], (g) S-rGO-0.25 [187]. Reprinted with the permission from Elsevier, Refs. [186–188,221]. (h–j) TEM images of (h) reduced graphene oxide (MRG), (i) B-doped MRG (B-MRG), and (j) high-resolution TEM image of B- and N-doped MRG (B-N-MRG). Reprinted with the permission from American Chemical Society, Ref. [170].

Analogous conditions were also used to obtain GO-based gelatin aerogels (Figure 10b,e) [221]. The binary aerogel was studied under acidic and alkaline conditions. Increasing the gelatin content in aerogel raises the modulus of elasticity to 6-fold and the swelling ratio up to 1.4-fold. The properties of the aerogel obtained using MW irradiation were compared with this synthesized using conventional heating. Similar physicochemical properties of both aerogels were identified; however, the swelling ratio value was 1.5 times higher for the aerogel synthesized using MW irradiation.

The following example shows the possibility of using the MW-assisted method to produce porous reduced graphene oxide (rGO) (Figure 10e,f) [188]. Conducting the synthesis

under MW irradiation conditions causes a shorter period and lower temperature, employing hydrochloric acid as an etching agent. In addition to lowering energy consumption, preparing the material under these conditions leads to obtaining material that avoids the restacking of subsequent rGO layers and numerous pores and promotes material transport efficiency. It is a critical phenomenon because reduced GO is characterized by a strong stacking effect of individual graphene layers, significantly limiting the potential of using this material in devices that accumulate electric charge. The combined macro/mesopore effect in porous rGO provides accessible ion transport pathways for the base electrolyte compared with conventionally prepared rGO. The electrochemical studies show that the synthesized rGO's calculated C_S was 568.5 F/g at 1 A/g with a remarkable capacity retention after longer charge/discharge cycles (Table 2).

An exciting example of using MW irradiation to modify GO is the method presented by Kwang S. Suh et al. [189]. The proposed facile and scalable method leads to the production of rGO by ionic liquid (IL)-assisted MW chemistry. ILs were used as sources of dipoles and the doping element rGO. The resulting material is characterized by the open porous architecture of rGO filled with IL moieties, resulting in easy ion transportation and consequently exhibiting a high C_S of 135 F/g. Additionally, a device operated at a voltage of 3.5 V revealed a high $E \sim 58$ Wh/kg and P amounting to 246 kW/kg.

MW radiation can easily be adapted to modify the graphene structure so that the carbon atoms in the graphene layer are replaced with other heteroatoms, such as N, S, P, or B [118,119,187] (please see Table 2). Deepak K. Pattanayak and coworkers presented an interesting example in 2020 (Figure 10d) [118]. Using a one-pot MW-assisted synthesis resulted in the doping of graphene with a high amount of N and S atoms (N,S-GO). The CN's heteroatom content, at 14.9% of N and 4.3% of S, leads to very high C_S values of 310 F/g in two electrodes symmetric configuration (1 M H_2SO_4 electrolyte). N,S-GO was also used in non-aqueous organic and IL electrolytes, where N,S-GO shows C_S of 226 F/g and 150 F/g with an energy density of 32 Wh/kg, respectively. The explanation of the heteroatom-doped graphene layer and the effect on the change of physical properties are described in detail in Section 3. Here, we will limit ourselves to discussing only some literature examples of preparing this doped structure.

Doping heteroatoms are an effective way to modify the physical properties of rGO. The modification of rGO using MW-assisted synthesis was applied to prepare S-doped rGO with different concentrations of S (Figure 10g) [187]. The synthesis was performed in mild experimental conditions at 140 °C for 30 min, which led to the wrinkling and folding of graphene sheets. The material with the highest content of S shows excellent electrochemical performance. A 5-fold increase in the number of sulfur atoms in the graphene sheets leads to a rise in the value from 61.7 to 237.6 F/g. The synthesized material has a promising potential for SC applications with simultaneous high electrochemical stability and capacitance retention of 106% after 10,000 cycles.

MW-assisted synthesis was also used to prepare B- and N-doped; and B,N-doped rGO (Figure 10h-j) [170]. The synthesized material possesses electromagnetic interference (EMI) shielding properties and high electrical conductivity. B,N-doped rGO shows high electrical conductivity compared with other materials: rGO, N-doped rGO, and B-doped rGO, which results in better EMI shielding ability. A high EMI shielding of -42 dB ($\sim 99.99\%$ attenuation) for B,N-doped rGO was measured compared with undoped rGO (-28 dB). The electrical conductivity increases from 21.4 (rGO) to 124.4 S/m (B,N-doped rGO) due to the nanojunction inside the material. The electrical conductivity depends on the temperature. In a low-temperature range ($T < 50$ K), the mechanism of the electrical conductivity is based on 2D-variable range hopping and the Efros-Shklovskii-VRH conduction model.

ND powders with different average particle sizes (10 nm to 1 μ m) are sensitive to MWs between 2.49 and 9.43 GHz [223]. Increased permittivity with decreasing particle size, polarization, and MW loss has already been observed. The oxygenation and hydrogenation of the NDs (sp^2 -hybridization was raised in the sample) led to dielectric polarization, and the loss increased [172]. Various methods have been applied to increase the heating

rate further and induce demanding reaction conditions. For example, specific substances, coating (MW-transparent substrates) or triggers have been added to tune the reaction conditions [167,169,172]. Using NDs in the environment of conducting polymers (ND-polyaniline) in MW-assisted synthesis significantly enhanced the MW absorption due to additional and intense polarization originating from the HN-CO groups acting as asymmetric centers [173]. These studies showed that ND particles might be applied as MW absorbers.

In some cases, such synthesis may require the addition of easily polarizing substances to tune the reaction conditions and to increase temperature. MW-assisted synthesis was also applied for the preparation of onion-like structures in the heavy crude oil and carbon catalyst (activated carbon and NiO-MoO₃/γ-Al₂O₃; 1:1 *w/w*) and tomatoes/carrots as a source of carbon and 30% NaOH [224,225]. The obtained CNs were non-homogenous with structural imperfections and an empty core; their structure did not resemble ND-derived CNOs.

The MW-assisted method was also successfully used to prepare and modify other CNs. An IL-assisted splitting method using MW irradiation as an external energy source produced graphene nanoribbons from MWCNT or SWCNT [226]. The process was based on two strategies: oxidation with strong acids and reduction with hydrazine. The MW-assisted method leads to splitting and expanding tubular graphite nanofibers, which consequently results in the preparation of graphene nanoribbons in the hundred nanometers. The MW-assisted synthesis was employed to prepare CNTs from acetylene and hydrogen as precursor gases [227]. The obtained CNTs were used as a sorbent to remove crystal violet. The sorption capacity was 81% upon contact with the analyte for 25 min at pH 7.0 using a sorbent concentration of 10 mg/L.

Using MW irradiation, it was possible to modify the tube walls in such a way as to remove the capped parts of the CNTs (Figure 2 and Table 2) [106]. The morphology of the CNTs was controlled by adjusting the MW powers. MW irradiation led to the opening of the nanotubes and the removal of fragments of the outer layers of CNTs. Moreover, it led to the formation of sp³-hybridized defects in the nanostructure. Such a modified structure of CNTs may facilitate the tunneling of electrons through the barriers and increase emission at new active sites.

MW-assisted synthesis was applied to grow N-CQDs on the surface of MWCNTs [218]. In conventional methods, N-CQDs are incorporated into the MWCNT surface by multistep processes, including the synthesis of the N-CQDs, their complex purification, surface activation, and crosslinking with the MWCNT surface. The method is simplified using MW irradiation by direct MW-assisted growth of N-CQDs on the MWCNT surface. Additionally, this surface modification method of MWCNTs effectively modulated their surface reactivity and internal band structure, which has a significant impact when studying electrocatalytic and photovoltaic processes. Based on the hybrid N-CQDs/MWCNT material, the dye-sensitized solar cells showed 50% higher photovoltaic efficiency than MWCNTs.

MW irradiation was applied to synthesizing composite containing GO and graphitic carbon nitride (g-C₃N₄), and the material's photocatalytic activity was tested [190]. A 12-fold increase in the photocatalytic efficiency of GO/g-C₃N₄ under visible light irradiation (224.6 μmol/h) in the production of H₂ compared with g-C₃N₄ was observed (Table 2). This effect is due to the ability of GO to accept and transport electrons from the excited g-C₃N₄, which significantly influenced the phenomenon of charge separation. The studies show the promising potential of this nanocomposite for electron collectors in photocatalytic H₂ production.

Gengchao Wang et al. presented an example of MW irradiation, where N-doped porous graphene frameworks were synthesized [192]. It is another example of creating a composite of graphene and CQDs (Table 2). An N-doped porous graphene framework is synthesized quickly during several processes running simultaneously. A readily dispersible graphene was an effective receptor for MW absorption and initiated GO reduction. Next, as an MW absorbing receptor, the reduced part of GO reduces the chain and allows N-doped porous graphene framework formation. The synthesized material has an outstanding

electrochemical performance and a volumetric absorption capacity that can be used in catalysis, energy storage, and environmental protection (Table 2). The electrodes made of GO/g-C₃N₄ delivered a volumetric E of 12.3 mWh/cm³ at P of 0.42 W/cm³. The N-doped porous graphene frameworks exhibited an extremely high volumetric absorption capacity of 100–243 g/cm³ for different oils and organic solvents.

These studies showed that CNs might be applied as MW absorbers in MW-assisted synthesis. In some cases, such synthesis may require the addition of easily polarizing substances to tune the reaction conditions and to increase the temperature to achieve the activation energy of a chemical reaction. Optimizing these parameters allows for the synthesis or modification of the CNs quickly.

4.3. MW-Assisted Synthesis for the Preparation of Hybrid Materials Containing d-CNs: Implications on Properties and Applications

MW irradiation is also a precious energy source for the preparation of multicomponent systems, often when conventional synthesis is highly complicated due to its multi-stage nature and the product purification being time-consuming. In addition, it is possible to conduct the synthesis in different experimental conditions, such as in the presence of a solvent or the solid phase, in ILs or using materials of various origins, including inorganic and organic. Combining materials into larger supramolecular systems or composites is simple by using MW irradiation due to a short time and low energy consumption.

An ultrafast MW process allows the synthesis of a carbon composite with the ordered mesoporous carbon as the core and CNT as the shell [68]. A 10–30 s MW irradiation catalyzes in situ CNTs growth within the nanochannel of ordered mesoporous carbon (Table 2). The whisker morphology of the obtained composite looks like a rambutan. Such interconnection between CNTs and mesoporous carbon particles effectively bridges 3D conducting networks, promoting the ion adsorption and diffusion of the supporting electrolyte. A composite consisting of a copolymer and CNTs was also prepared [228]. The oxidized CNTs were incorporated into the polymer matrix consisting of poly(*o*-phenylenediamine-co-aniline) using MW irradiation (for 45 min at intervals of 5 min) to accelerate the polymerization. The oxidation of CNTs was also supported by MW irradiation for 30 min at 160 °C. Combining these synthetic procedures led to the preparation of a composite with a needle-like structure of the copolymer. The system of the copolymer and nanocomposite enables the effective accumulation of electric charge. They exhibited a high C_S of 147.14 F/g at 0.50 A/g with a capacitance retention of 82%.

MW irradiation is more often used to combine materials of different chemical natures, mainly for the synthesis of composites containing CNs and metallic nanoparticles [197,204,205,211,213,229,230], nanopellets [212], or core-shell structures [194–196]. Metallic nanoparticles can, of course, consist only of pristine metallic nanoparticles [211,214]; they can form metallic connections of various elements [194,195], metal hydroxide [231], metal oxides [185,232], nitride [207], or sulfides [197,210], in various combination, etc.

Since then, the worldwide studies of electrocatalytic processes have been dominated by precious-metal-based-materials: Pt-, Pd-, Mo-, Fe-, and Co-based catalysts for ORR and HER [233–235]. Au- and Ag-based catalysts for electrocatalytic CO₂ reduction reaction (CO₂RR) [236,237], and Ru- and Ir-based catalysts for OER [238,239]. Generally, metal-based catalysts are characterized by low selectivity, poor durability, and susceptibility to gas poisoning. Due to the cost and the scarcity of some metals, their practical and large-scale use still needs to be improved. Pt nanoparticles have long been regarded as the best catalyst for ORR. However, due to the notable disadvantages listed above, the commercialization of these technologies needs to be improved. Therefore, it is necessary to search for alternative earth-abundant materials. CNs demonstrate excellent electrocatalytic activity with high stability [37,81,240]. A new generation of electrocatalysts is developed, in which defective surface of materials promotes multiple-proton-coupled electron transfer and mass transportation [41]. In this context, combining materials of different chemical nature can optimize the properties of the designed materials.

The idea of using MW irradiation in composite preparation containing metallic nanoparticles and CNTs is schematically presented in Figure 11 [214]. In the first stage, CNs with metallic precursors and substances that are good MW absorbers are placed simultaneously in an MW reactor (Figure 11a). Graphene platelets in ILs and Pd acetate were mixed in this case. The impregnation and partial exfoliation of graphene happened due to MW irradiation and weak Van der Waal's and π - π interaction. The IL reduced the diameter of dissolved Pd cations. As a result, they created Pd nanoparticles, which were distributed on graphene sheets. At the same time, structural defects are formed in the graphene layer due to MW irradiation or the catalytic activity of the IL. These defects act as nucleation sites for core-shell structures of the Pd nanoparticles with imidazolium shells. During further MW irradiation, the outer organic layer decomposes, resulting in it being formed carbonaceous gasses. These are carbon sources for CNT growth. Carbon diffuses on the Pd nanoparticle's surface and comprises multi-walled core-shell nanoparticles.

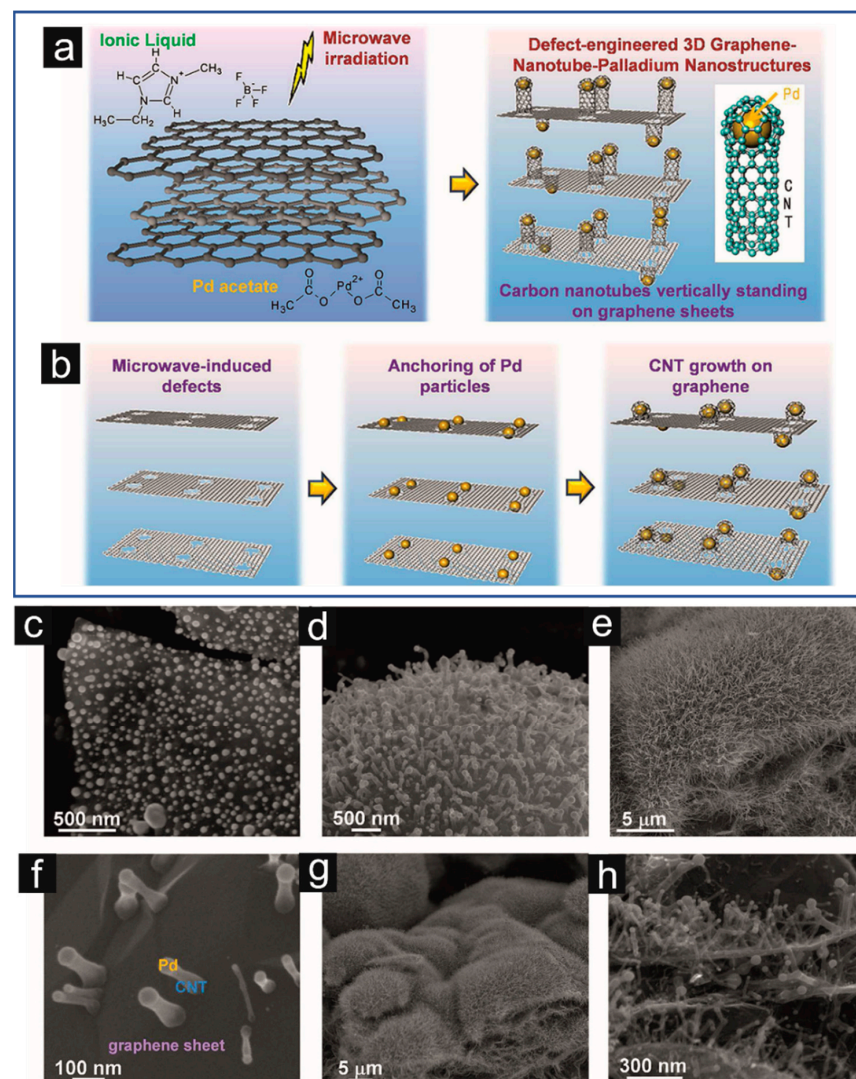


Figure 11. Schematic representation of one-pot MW synthesis of 3D carbon hybrid nanostructures showing vertically grown CNTs on graphene sheets: (a) scheme and (b) mechanism. (c–h) SEM images of 3D CNs showing CNTs vertically attached to graphene sheets: (c) Pd nanoparticles initially anchored on graphene, (d) vertically standing CNTs grown on graphene by Pd nanoparticles, (e) CNT forest extensively grown on graphene surfaces after lengthy MW irradiation, (f) direct bonding between CNTs and graphene, (g) mass production of 3D G-CNT-Pd nanostructures, and (h) terrace structures of hybrid material. Reprinted with the permission from American Chemical Society, Ref. [214].

It has to be noted that direct bonding between CNTs and graphene was detected due to the defect-based growth mechanism (Figure 11b). Under these conditions, a dense brush of CNTs with Pd nanoparticles placed perpendicularly to the graphene surface was performed (Figure 11d). By manipulating the amount of graphene used for Pd and MW irradiation power and time, the composition of the resulting hybrid material was quantitatively controlled (Figure 11e). In many cases, it is simplified, mainly when we want to get two-component composites with a random 3D organization. This type of functionalization was presented in works in which the carbonaceous component was graphene [211] and N-doped GO [230]. This process is illustrated in detail in Figure 3 and discussed in Section 4.2 [211]. The results show the 3D Pd-E-PG nanostructure has a ~ 5.4 wt. % H₂ storage capacity under 7.5 MPa and CO oxidation catalytic activity at 190 °C. The synthesized N-GO/Pd material was also used as a catalyst for ethanol electrooxidation with a j of 10 mA/cm² [230]. Analogous N-rGO/Pd material was used in direct-ethanol fuel cells [209]. The electrocatalytic activity of N-rGO/Pd was accessed by cyclic voltammetry (CV) in the presence of ethanol. The N-rGO/Pd catalyst exhibits better electrocatalytic performance than rGO/Pd, with an electroactive surface area of 6.3 m²/g and ~ 3.7 m²/g, respectively.

In addition to composites containing pure metallic nanoparticles and bimetallic nanoparticles, other compounds containing a metallic component are often synthesized (Table 2). Most commonly, this may include metal oxides [185,204,205,229,231,232], nitride [207], or sulfides [197,210], in various combinations, etc. MW-assisted synthesis is an effective method for the facile and fast preparation of hybrid materials. It is usually the last stage of the synthesis, often preceded by obtaining CNs or their initial modification. A good example is an article on preparing a composite containing MWCNTs and Fe₃O₄ (Table 2) [229]. The pristine MWCNTs and N-doped MWCNTs were formed using the CVD method. Next, the Fe₃O₄ nanoparticles (5–15 nm) were synthesized directly on the MWCNT surface in an MW-assisted process. The homogeneous distribution of nanoparticles on the surface of CNs, the formation of defects on the surface of MWCNTs during MW irradiation, and the doping of CNs with N improve the saturation magnetization of the resulting composites.

An MW irradiation was also used as an energy source to support the preparation of NiO [231], MnCo₂O₄ [204], and α -MoO₃ [205,208] (Table 2). Nanoparticles of metallic oxides were directly grown on graphene sheets using the in situ MW irradiation method. A periodic repetition of MW irradiation through several cycles significantly increases the efficiency of the synthesis reaction, leading to large-scale processes [208]. The multi-step preparation of sulfides [197,203,212,213] may also be simplified by using MW-hydrothermal preparation of nanoparticles. In this case, it is not necessary to use chemical surfactants, and the preparation time is significantly reduced from several days to a few minutes. The homogeneous distribution of CNs in solution was preceded by the partial exfoliation of graphene, which was carried out by MW irradiation. This approach ensured a homogeneous distribution of nanoparticles in the bulk of the composite. The nanoparticles were covered with graphene sheets or intercalated inside the materials. It, in turn, provides a conductive scaffold constructed from graphene sheets, increasing the material's specific surface area and chemical stability. Hybrid composites' porous and interconnected structures promote charge transport by encapsulating agglomerated metallic nanoparticles.

Using MW irradiation, it is also possible to obtain core-shell structures quickly [194–196]. In this case, the CNTs are surrounded by an inorganic phase, as shown in Figure 12a–d [194]. Briefly, in the first step, the oxidation of the MWCNTs was performed to increase their dispersibility and to introduce the nucleation sites for the inorganic nanoparticle creation. Next, a mixture of inorganic salt and an oxidizing agent was subjected to MW irradiation at elevated temperatures. Consequently, the walls of the MWCNTs were uniformly covered with an inorganic crystalline phase of various forms of crystallites. Depending on the irradiation power, temperature, or reaction time, the degree of coverage of MWCNTs varied. It is also possible to obtain a core-shell structure in the inorganic phase alone

(Figure 12f–i). Then, two phases with different crystal structures are distinguished [195]. CoMoO_4 nanopellets have a core-shell form with a well-crystallized bulk. The shell of CoMoO_4 crystallite is amorphous. In both cases, the oxidized CNTs were utilized as MW absorbers and heterogeneous nucleation sites for inorganic nanocrystal formation. The MWCNT/ CoMoO_4 composite used as an electrode in the capacitors shows a C_S of 170 F/g and a high cycling stability of 93.2% after 1000 cycles (Table 2) [195].

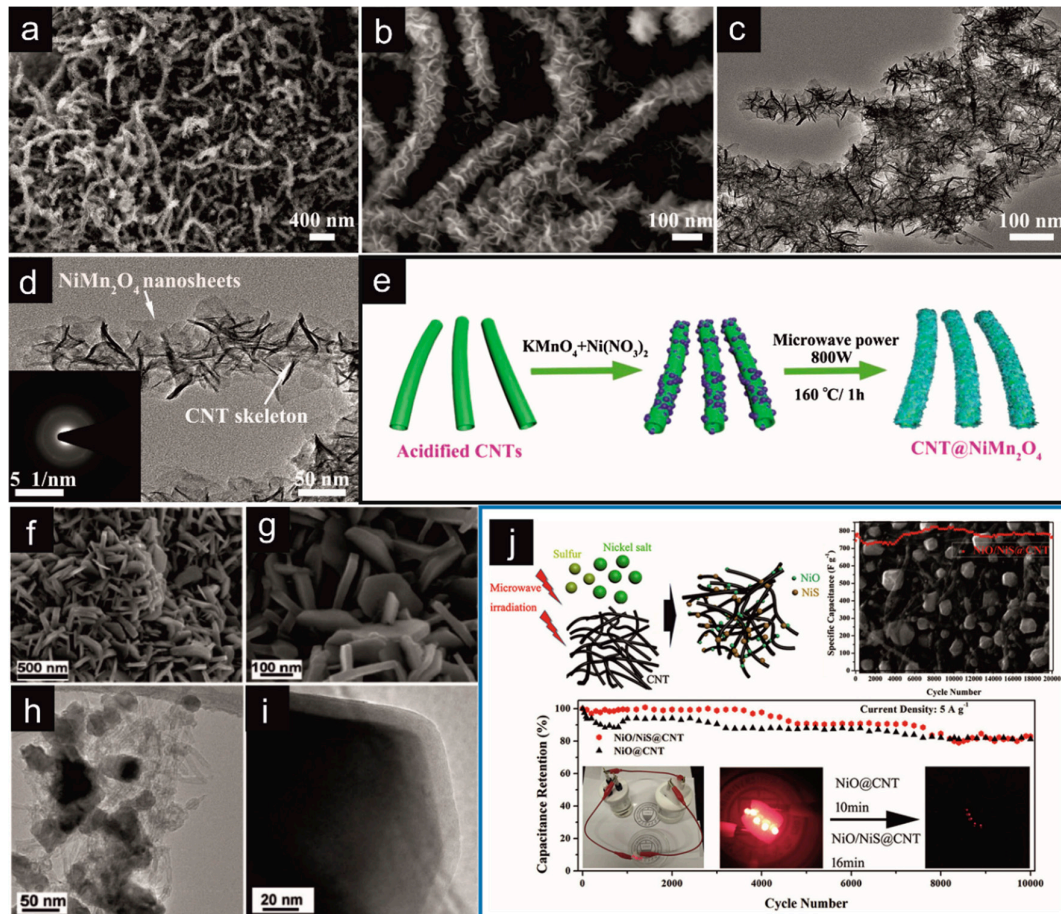


Figure 12. Schematic representation of the core-shell structures prepared by MW-assisted synthesis. (a,b) The low- and high-resolution FESEM images of CNT/ NiMn_2O_4 composite (c,d) TEM images of CNT/ NiMn_2O_4 composite; inset shows the selected area electron diffraction pattern. (e) Schematic representation of the formation of core-shell structures of the CNT/ NiMn_2O_4 composite. Reprinted with the permission of Elsevier from Ref. [194]. (f,g) SEM and (h) TEM images of MWCNT/ CoMoO_4 . (i) TEM image of individual CoMoO_4 crystallite (core-shell structure). Reprinted with the permission from RSC, Ref. [195]. (j) Schematic illustration of the formation of NiS@CNT/NiO nanocomposites. SEM image of NiS@CNT/NiO . Reprinted with the permission from Elsevier, Ref. [196].

The CNT/ NiMn_2O_4 composite synthesized by an MW-assisted hydrothermal process exhibited excellent electrochemical performance [194]. The electrochemical studies performed for these materials are shown in Figure 13. The CNT/ NiMn_2O_4 electrode exhibits a high C_S of up to 915.6 F/g at 1 A/g and an excellent cycling stability of 93.0% after 5000 cycles at 5 A/g. These properties are affected by the weaker crystallinity of NiMn_2O_4 and more defects and vacancies in CNTs. The CV curves exhibit similar electrochemical characteristics in the potential window from 1.3 to 1.6 V (Figure 13c). Increasing the voltage to 1.7 V and the OER and HER cause a jump in the charge current. It should be noted that the shape of the charge-discharge curves shows good linearity and symmetry in the potential range of 1.3–1.6 V (1.5 A/g), indicating the reversibility of the processes (Figure 13d).

An asymmetric SC device with a positive electrode composed from CNT/NiMn₂O₄ shows the maximum energy density of 36.5 Wh/kg at P of 800 W/kg and cycling stability of 82.8% after 10,000 cycles at 5 A/g (Figure 13i). These parameters are higher than for other SC devices based on NiMn.

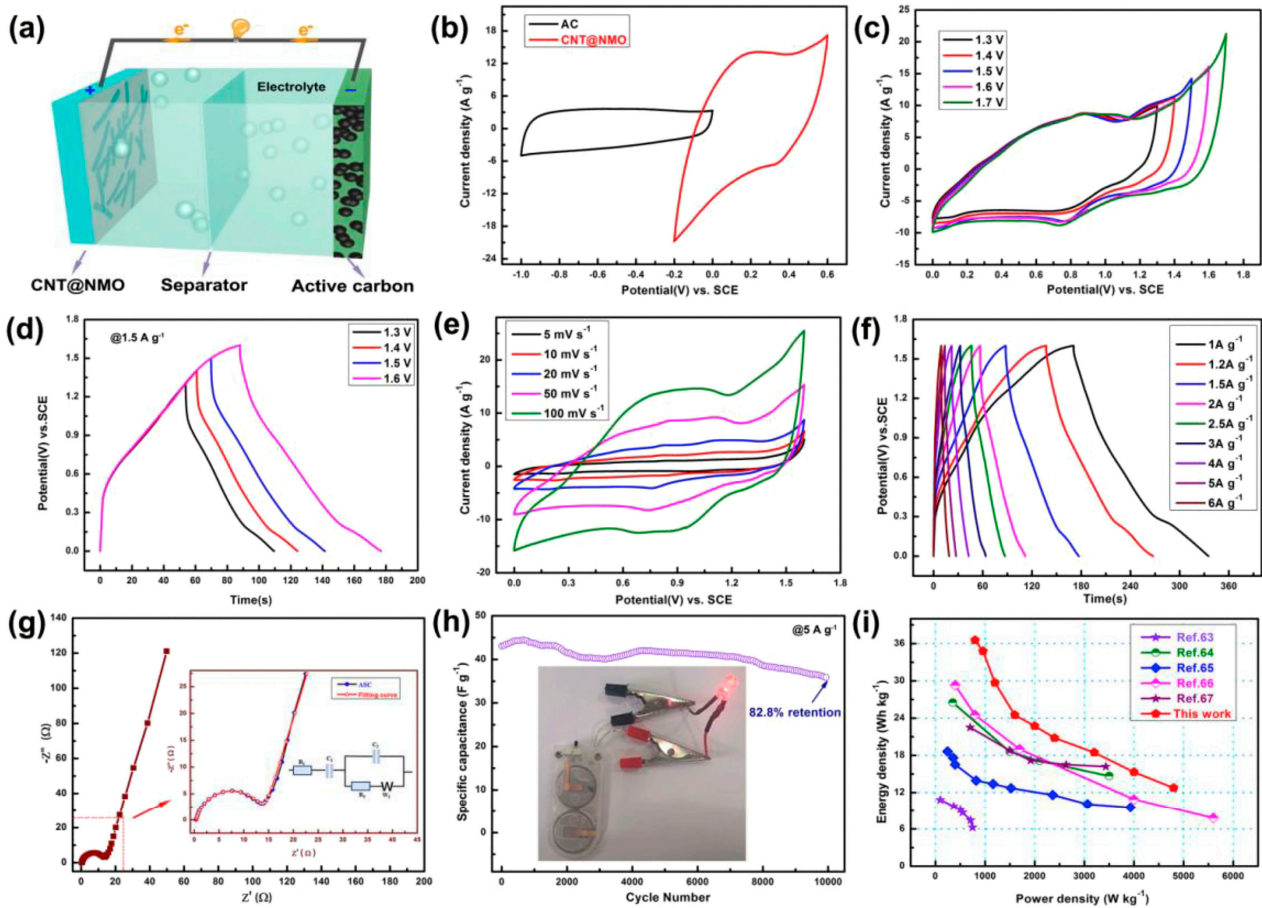


Figure 13. (a) Schematic diagram of CNT/NiMn₂O₄ asymmetric supercapacitor device. (b) Comparative CV curves of AC CNT/NiMn₂O₄ electrodes in a three-electrode system, 50 mV/s. (c) CVs of the device were measured at different potential windows, 50 mV/s. (d) The charge/discharge curves of the device were measured at different potential windows at 1.5 A/g. (e) CVs at the different scan rates from 0 to 1.6 V. (f) The charge/discharge curves measured at different current densities. (g) Electrochemical impedance spectra of the device. (h) Cyclic performance of the device at 5 A/g for 10,000 cycles. (i) The Ragone plots of the CNT/NiMn₂O₄ and comparison with literature data. Reprinted with the permission from Elsevier, Ref. [194].

A multi-component nanocomposite consisting of CNTs, NiO, and NiS (NiS@CNT/NiO) was prepared quickly (60 s) using a one-step MW-assisted method (please see Table 2, Figure 12j) [196]. The different mass ratios of used substrates and MW conditions performed in the reaction were tested for their influence on the electrochemical properties of the created material. The composites containing both inorganic components, NiS, and NiO, showed optimal electrochemical performance. The NiS@CNT/NiO electrodes showed a C_S of 809.7 F/g at 1 A/g and a cycling stability of approximately 100% retention after 20,000 cycles at 5 A/g. In the following example, MW-assisted hydrothermal synthesis was used to prepare the composite containing NiS and rGO (rGO/NiS) [197]. The MW-assisted synthesis eliminates chemical surfactants and reduces the preparation time from several days to only 6 h [197]. The electrodes fabricated from rGO/NiS exhibit an ultrahigh C_S of 1745.7 F/g at 1 A/g and a high-capacity retention after 3000 cycles with high reproducibility.

The symmetric solid-state SC shows a C_S of 14.20 F/g, an E of 7.1 Wh/kg and a P of 1836 W/kg (Table 2). The SC device based on N-rGO/NiS exhibits similar electrochemical performance with a C_S of 1467.8 F/g at 1 A/g [203]. An asymmetric configuration of the capacitor, where N-rGO//N-rGO/NiS and graphite sheet as the current collector was used, characterizes the following parameters: a cyclic stability of 86.6% after 5000 cycles and an E of 66.6 Wh/kg and a P of 405.83 W/kg. Due to these parameters, the hybrid materials show potential for energy-storage applications.

The 3D S-rGO/NiFeS₂ composite was synthesized using a one-step MW alcohol-thermal method, in which mercaptoacetic acid is used as a sulfur source for the doping of graphene and as a precursor of nickel-iron sulfide (Table 2) [210]. The composite shows a very porous structure and a large SSA, and thanks to chemical bonds with sulfur, it increases the binding of the nickel-iron precursor to the carbon material. These phenomena ensure the C_S value of 1073.2 F/g at 1 A/g in 6.0 M KOH electrolyte. The asymmetric SC device, operating in the range of 1.6 V, delivers. The hybrid materials containing CN and Ni components show potential for energy-storage applications.

Simonkolleite (Zn₅(OH)₈Cl₂·H₂O) nanoplatelets were deposited on nickel foam-supported graphene (NiF-G/SimonK) using an MW-assisted hydrothermal method (Table 2) [212]. In this condition, the porous NiF-G/SimonK composite was obtained, in which the structural and morphological characteristic significantly affects the electrochemical performance. The NiF-G/SimonK composite, used as electrodes, exhibits a C_S of 836 F/g at a j of 1 A/g and a cycling stability with capacitance retention of 92% after 5000 charge/discharge cycles. An MW-assisted synthesis was used to prepare a honeycomb-like graphene/NiCoS (G/NiCoS) composite [213]. The defect-rich structures of G/NiCoS ensure excellent electrochemical properties of this composite. The device with the electrodes made of G/NiCoS exhibits a high C_S of 1186 F/g at 1 A/g and a capacity of 89.2% after 10,000 cycles, and an E of 46.4 Wh/kg. Due to their high energy and power density and excellent cycling stability, the multi-component hybrid materials show potential for energy-storage applications and electrocatalysis.

5. Concluding Remarks

The electrochemical properties of carbon-based electrode materials are closely related to their chemical composition, structure, and defects. They are ideal for catalysis, electrocatalysis, and electrochemistry due to their excellent conductivity and mechanical stability, sizeable specific area with micro- and mesoporosity, easy production, and high charged carrier mobility. They are also good candidates for electrocatalysis due to the easy formation of the defects in their networks that affect decreasing the reaction kinetic barriers while simultaneously increasing the efficiency and selectivity of the chemical transformation involved. From a chemical point of view, the essence of catalysis is breaking and re-forming chemical bonds under the influence of an external force. The ability to create carbon-carbon or carbon-heteroatom bonds in a simple way allows the use of this property, for example, in the production of fuels (H₂ and O₂).

Since all these parameters are easily achievable during the creation or modification of CNs, including during the irradiation of MW substrates, it is becoming increasingly used in this area. It was determined that not only the simplicity, reaction time, and the possibility of conducting it both in solution and the solid phase led to this, but above all the possibility of combining substrates of different chemical natures. Despite the many advantages of carbon-based materials, in some cases, it is necessary to combine them, for example, with an inorganic component, to achieve optimal final parameters. Also, in this respect, MW irradiation is an excellent source of energy that activates the chemical reaction between the organic and inorganic phases. The obtained materials have a homogeneous form because, as mentioned earlier, MW-assisted synthesis can be carried out in the solid phase, where the problem of solubility of organic and inorganic compounds in a given solvent is eliminated. Finally, the possibility of various combinations of synthesis parameters and substrates makes MW-assisted synthesis a universal method.

The review indicated that it is possible to create multi-component materials thanks to MW-assisted synthesis. Not only is it easy and quick to combine inorganic and carbonaceous materials, but often, the resulting materials exhibit unique structures and morphologies that need to be more attainable using conventional methods. Their physical and chemical properties make using them in many scientific fields possible. Here, we focused mainly on the electrochemical and electrocatalytic properties of the obtained materials because, in these areas, new solutions are constantly being sought to produce materials with optimal parameters. Because current scientific research indicates that in electrochemical and electrocatalytic processes of carbon-based materials, not only the surface morphology has a significant impact on the effectiveness of these reactions but also the heterogeneity of the structure; therefore, MW-assisted synthesis is considered one of the most promising methods in this area. Unfortunately, many of the solutions presented in this review still need to meet the parameters desired on an industrial scale.

When we think about industrial applications, we think about more than just the macro scale, which is often difficult to achieve, e.g., due to the kinetics of chemical reactions in large volumes. In this regard, we also need to take other factors into account. These certainly include the ease of producing materials, i.e., the simplicity of the technological process, the removal of intermediate products from the reaction mixture, limitations in using organic solvents, and low energy inputs in the entire technological process. All these parameters shape the product's final price, i.e., in our case, a material with specific electrochemical and electrocatalytic properties. MW-assisted synthesis meets all the above assumptions and enables simple and cheap chemical reactions to achieve the intended synthesis goal. The examples of creating hybrid materials using MW irradiation presented here have great potential, and this trend should be developed in the future. However, the literature data presented are still within the scope of basic research, indicating that the transition from the micro- to macroscale is still a milestone.

Author Contributions: Conceptualization, M.E.P.-B.; writing—original draft preparation, D.P. and M.E.P.-B.; writing—review and editing, M.E.P.-B.; visualization, D.P. and M.E.P.-B.; supervision, M.E.P.-B.; project administration, M.E.P.-B.; funding acquisition, M.E.P.-B. All authors have read and agreed to the published version of the manuscript.

Funding: We gratefully acknowledge the financial support of the National Science Centre, Poland, grant #2019/35/B/ST5/00572 to M.E.P.-B.

Institutional Review Board Statement: Not applicable.

Informed Consent Statement: Not applicable.

Data Availability Statement: 3rd Party Data.

Conflicts of Interest: The authors declare no conflict of interest.

References

1. Gu, W.; Yushin, G. Review of Nanostructured Carbon Materials for Electrochemical Capacitor Applications: Advantages and Limitations of Activated Carbon, Carbide-Derived Carbon, Zeolite-Templated Carbon, Carbon Aerogels, Carbon Nanotubes, Onion-like Carbon, and Graphene: Nanostructured Carbon Materials for Electrochemical Capacitor Applications. *Wiley Interdiscip. Rev. Energy Environ.* **2014**, *3*, 424–473. [[CrossRef](#)]
2. Al-Jumaili, A.; Alancherry, S.; Bazaka, K.; Jacob, M. Review on the Antimicrobial Properties of Carbon Nanostructures. *Materials* **2017**, *10*, 1066. [[CrossRef](#)] [[PubMed](#)]
3. Bobrowska, D.M.; Olejnika, P.; Echevoyen, L.; Brzezinska, M. Onion-like Carbon Nanostructures: An Overview of Bio-Applications. *Curr. Med. Chem.* **2018**, *25*, 6896–6914. [[CrossRef](#)] [[PubMed](#)]
4. Yu, S.-S.; Zheng, W.-T. Effect of N/B Doping on the Electronic and Field Emission Properties for Carbon Nanotubes, Carbon Nanocones, and Graphene Nanoribbons. *Nanoscale* **2010**, *2*, 1069. [[CrossRef](#)] [[PubMed](#)]
5. Rathinavel, S.; Priyadharshini, K.; Panda, D. A Review on Carbon Nanotube: An Overview of Synthesis, Properties, Functionalization, Characterization, and the Application. *Mater. Sci. Eng. B* **2021**, *268*, 115095. [[CrossRef](#)]
6. Robertson, J. Comparison of Diamond-like Carbon to Diamond for Applications. *Phys. Status Solidi A* **2008**, *205*, 2233–2244. [[CrossRef](#)]
7. Robertson, J. Electronic Structure of Diamond-like Carbon. *Diam. Relat. Mater.* **1997**, *6*, 212–218. [[CrossRef](#)]

8. Mykhailiv, O.; Zubyk, H.; Plonska-Brzezinska, M.E. Carbon Nano-Onions: Unique Carbon Nanostructures with Fascinating Properties and Their Potential Applications. *Inorganica Chim. Acta* **2017**, *468*, 49–66. [[CrossRef](#)]
9. Yang, G.; Li, L.; Lee, W.B.; Ng, M.C. Structure of Graphene and Its Disorders: A Review. *Sci. Technol. Adv. Mater.* **2018**, *19*, 613–648. [[CrossRef](#)]
10. Gao, X.; Liu, H.; Wang, D.; Zhang, J. Graphdiyne: Synthesis, Properties, and Applications. *Chem. Soc. Rev.* **2019**, *48*, 908–936. [[CrossRef](#)]
11. Khan, K.; Tareen, A.K.; Iqbal, M.; Shi, Z.; Zhang, H.; Guo, Z. Novel Emerging Graphdiyne Based Two Dimensional Materials: Synthesis, Properties and Renewable Energy Applications. *Nano Today* **2021**, *39*, 101207. [[CrossRef](#)]
12. Zhao, Y.; Yang, N.; Yu, R.; Zhang, Y.; Zhang, J.; Li, Y.; Wang, D. Unique Structural Advances of Graphdiyne for Energy Applications. *EnergyChem* **2020**, *2*, 100041. [[CrossRef](#)]
13. Liu, H.; Zhang, L.; Yan, M.; Yu, J. Carbon Nanostructures in Biology and Medicine. *J. Mater. Chem. B* **2017**, *5*, 6437–6450. [[CrossRef](#)]
14. Hu, Y.; Shenderova, O.A.; Hu, Z.; Padgett, C.W.; Brenner, D.W. Carbon Nanostructures for Advanced Composites. *Rep. Prog. Phys.* **2006**, *69*, 1847–1895. [[CrossRef](#)]
15. Kumar, S.; Rani, R.; Dilbaghi, N.; Tankeshwar, K.; Kim, K.-H. Carbon Nanotubes: A Novel Material for Multifaceted Applications in Human Healthcare. *Chem. Soc. Rev.* **2017**, *46*, 158–196. [[CrossRef](#)] [[PubMed](#)]
16. Sek, S.; Brezczko, J.; Plonska-Brzezinska, M.E.; Wilczewska, A.Z.; Echegoyen, L. STM-Based Molecular Junction of Carbon Nano-Onion. *ChemPhysChem* **2013**, *14*, 96–100. [[CrossRef](#)] [[PubMed](#)]
17. Wang, M.-S.; Golberg, D.; Bando, Y. Carbon “Onions” as Point Electron Sources. *ACS Nano* **2010**, *4*, 4396–4402. [[CrossRef](#)] [[PubMed](#)]
18. Keller, N.; Maksimova, N.I.; Roddatis, V.V.; Schur, M.; Mestl, G.; Butenko, Y.V.; Kuznetsov, V.L.; Schlögl, R. The Catalytic Use of Onion-like Carbon Materials for Styrene Synthesis by Oxidative Dehydrogenation of Ethylbenzene. *Angew. Chem. Int. Ed. Engl.* **2002**, *41*, 1885–1888. [[CrossRef](#)]
19. Su, D.; Maksimova, N.I.; Mestl, G.; Kuznetsov, V.L.; Keller, V.; Schlögl, R.; Keller, N. Oxidative Dehydrogenation of Ethylbenzene to Styrene over Ultra-Dispersed Diamond and Onion-like Carbon. *Carbon* **2007**, *45*, 2145–2151. [[CrossRef](#)]
20. Feng, Y.; Jiang, J.; Xu, Y.; Wang, S.; An, W.; Chai, Q.; Prova, U.H.; Wang, C.; Huang, G. Biomass Derived Diverse Carbon Nanostructure for Electrocatalysis, Energy Conversion and Storage. *Carbon* **2023**, *211*, 118105. [[CrossRef](#)]
21. Plonska-Brzezinska, M.E.; Echegoyen, L. Carbon Nano-Onions for Supercapacitor Electrodes: Recent Developments and Applications. *J. Mater. Chem. A* **2013**, *1*, 13703. [[CrossRef](#)]
22. Lee, J.; Lee, T.H.; Jang, H.W.; Park, H.S. Chemical Modification of Ordered/Disordered Carbon Nanostructures for Metal Hosts and Electrocatalysts of Lithium-Air Batteries. *InfoMat* **2022**, *4*, e12268. [[CrossRef](#)]
23. Bobrowska, D.M.; Brzezinski, K.; Echegoyen, L.; Plonska-Brzezinska, M.E. A New Perspective on Carbon Nano-Onion/Nickel Hydroxide/Oxide Composites: Physicochemical Properties and Application in Hybrid Electrochemical Systems. *Fuller. Nanotub. Carbon Nanostruct.* **2017**, *25*, 193–203. [[CrossRef](#)]
24. Luszczyn, J.; Plonska-Brzezinska, M.E.; Palkar, A.; Simionescu, A.; Simionescu, D.T.; Kalska-Szostko, B.; Winkler, K.; Echegoyen, L. Small Noncytotoxic Carbon Nano-Onions: First Covalent Functionalization with Biomolecules. *Chem. Eur. J.* **2010**, *16*, 4870–4880. [[CrossRef](#)]
25. Brezczko, J.; Plonska-Brzezinska, M.E.; Echegoyen, L. Electrochemical Oxidation and Determination of Dopamine in the Presence of Uric and Ascorbic Acids Using a Carbon Nano-Onion and Poly(Diallyldimethylammonium Chloride) Composite. *Electrochim. Acta* **2012**, *72*, 61–67. [[CrossRef](#)]
26. Huang, Y.; Liang, J.; Chen, Y. The Application of Graphene Based Materials for Actuators. *J. Mater. Chem.* **2012**, *22*, 3671. [[CrossRef](#)]
27. Sohoul, E.; Ghalkhani, M.; Zargar, T.; Joseph, Y.; Rahimi-Nasrabadi, M.; Ahmadi, F.; Plonska-Brzezinska, M.E.; Ehrlich, H. A New Electrochemical Aptasensor Based on Gold/Nitrogen-Doped Carbon Nano-Onions for the Detection of Staphylococcus aureus. *Electrochim. Acta* **2022**, *403*, 139633. [[CrossRef](#)]
28. Bobrowska, D.M.; Brzezinski, K.; Plonska-Brzezinska, M.E. PEGylated Carbon Nano-Onions Composite as a Carrier of Polyphenolic Compounds: A Promising System for Medical Applications and Biological Sensors. *Colloid Interface Sci. Commun.* **2017**, *21*, 6–9. [[CrossRef](#)]
29. Banerjee, A.N. Graphene and Its Derivatives as Biomedical Materials: Future Prospects and Challenges. *Interface Focus* **2018**, *8*, 20170056. [[CrossRef](#)]
30. Bartelmess, J.; Giordani, S. Carbon Nano-Onions (Multi-Layer Fullerenes): Chemistry and Applications. *Beilstein J. Nanotechnol.* **2014**, *5*, 1980–1998. [[CrossRef](#)]
31. Ghosh, M.; Sonkar, S.K.; Saxena, M.; Sarkar, S. Carbon Nano-Onions for Imaging the Life Cycle of Drosophila Melanogaster. *Small* **2011**, *7*, 3170–3177. [[CrossRef](#)] [[PubMed](#)]
32. Giordani, S.; Bartelmess, J.; Frascioni, M.; Biondi, I.; Cheung, S.; Grossi, M.; Wu, D.; Echegoyen, L.; O’Shea, D.F. NIR Fluorescence Labelled Carbon Nano-Onions: Synthesis, Analysis and Cellular Imaging. *J. Mater. Chem. B* **2014**, *2*, 7459–7463. [[CrossRef](#)] [[PubMed](#)]
33. Regulska, E.; Olejnik, P.; Zubyk, H.; Czyrko-Horczak, J.; Chaur, M.N.; Tomczykowa, M.; Butsyk, O.; Brzezinski, K.; Echegoyen, L.; Plonska-Brzezinska, M.E. Nanostructural Catalyst: Metallophthalocyanine and Carbon Nano-Onion with Enhanced Visible-Light Photocatalytic Activity towards Organic Pollutants. *RSC Adv.* **2020**, *10*, 10910–10920. [[CrossRef](#)] [[PubMed](#)]

34. Mykhailiv, O.; Brzezinski, K.; Sulikowski, B.; Olejniczak, Z.; Gras, M.; Lota, G.; Molina-Ontoria, A.; Jakubczyk, M.; Echegoyen, L.; Plonska-Brzezinska, M.E. Boron-Doped Polygonal Carbon Nano-Onions: Synthesis and Applications in Electrochemical Energy Storage. *Chem. Eur. J.* **2017**, *23*, 7132–7141. [[CrossRef](#)] [[PubMed](#)]
35. Simon, P.; Gogotsi, Y. Materials for Electrochemical Capacitors. *Nat. Mater.* **2008**, *7*, 845–854. [[CrossRef](#)] [[PubMed](#)]
36. Li, D.; Jia, Y.; Chang, G.; Chen, J.; Liu, H.; Wang, J.; Hu, Y.; Xia, Y.; Yang, D.; Yao, X. A Defect-Driven Metal-Free Electrocatalyst for Oxygen Reduction in Acidic Electrolyte. *Chem* **2018**, *4*, 2345–2356. [[CrossRef](#)]
37. Jiang, Y.; Yang, L.; Sun, T.; Zhao, J.; Lyu, Z.; Zhuo, O.; Wang, X.; Wu, Q.; Ma, J.; Hu, Z. Significant Contribution of Intrinsic Carbon Defects to Oxygen Reduction Activity. *ACS Catal.* **2015**, *5*, 6707–6712. [[CrossRef](#)]
38. Tang, C.; Wang, H.-F.; Chen, X.; Li, B.-Q.; Hou, T.-Z.; Zhang, B.; Zhang, Q.; Titirici, M.-M.; Wei, F. Topological Defects in Metal-Free Nanocarbon for Oxygen Electrocatalysis. *Adv. Mater.* **2016**, *28*, 6845–6851. [[CrossRef](#)]
39. Banham, D.; Ye, S.; Pei, K.; Ozaki, J.; Kishimoto, T.; Imashiro, Y. A Review of the Stability and Durability of Non-Precious Metal Catalysts for the Oxygen Reduction Reaction in Proton Exchange Membrane Fuel Cells. *J. Power Sources* **2015**, *285*, 334–348. [[CrossRef](#)]
40. Zheng, Y.; Jiao, Y.; Zhu, Y.; Cai, Q.; Vasileff, A.; Li, L.H.; Han, Y.; Chen, Y.; Qiao, S.-Z. Molecule-Level g-C₃N₄ Coordinated Transition Metals as a New Class of Electrocatalysts for Oxygen Electrode Reactions. *J. Am. Chem. Soc.* **2017**, *139*, 3336–3339. [[CrossRef](#)]
41. Jia, Y.; Jiang, K.; Wang, H.; Yao, X. The Role of Defect Sites in Nanomaterials for Electrocatalytic Energy Conversion. *Chem* **2019**, *5*, 1371–1397. [[CrossRef](#)]
42. Yan, X.; Jia, Y.; Yao, X. Defects on Carbons for Electrocatalytic Oxygen Reduction. *Chem. Soc. Rev.* **2018**, *47*, 7628–7658. [[CrossRef](#)] [[PubMed](#)]
43. Chung, H.T.; Cullen, D.A.; Higgins, D.; Sneed, B.T.; Holby, E.F.; More, K.L.; Zelenay, P. Direct Atomic-Level Insight into the Active Sites of a High-Performance PGM-Free ORR Catalyst. *Science* **2017**, *357*, 479–484. [[CrossRef](#)] [[PubMed](#)]
44. Zhou, H.; Sheng, X.; Xiao, J.; Ding, Z.; Wang, D.; Zhang, X.; Liu, J.; Wu, R.; Feng, X.; Jiang, L. Increasing the Efficiency of Photocatalytic Reactions via Surface Microenvironment Engineering. *J. Am. Chem. Soc.* **2020**, *142*, 2738–2743. [[CrossRef](#)] [[PubMed](#)]
45. Bai, S.; Jiang, W.; Li, Z.; Xiong, Y. Surface and Interface Engineering in Photocatalysis. *ChemNanoMat* **2015**, *1*, 223–239. [[CrossRef](#)]
46. Li, J.; Abbas, S.U.; Wang, H.; Zhang, Z.; Hu, W. Recent Advances in Interface Engineering for Electrocatalytic CO₂ Reduction Reaction. *Nano-Micro Lett.* **2021**, *13*, 216. [[CrossRef](#)] [[PubMed](#)]
47. Chen, S.; Liu, X.; Xiong, J.; Mi, L.; Song, X.-Z.; Li, Y. Defect and Interface Engineering in Metal Sulfide Catalysts for the Electrocatalytic Nitrogen Reduction Reaction: A Review. *J. Mater. Chem. A* **2022**, *10*, 6927–6949. [[CrossRef](#)]
48. Mykhailiv, O.; Zubyk, H.; Brzezinski, K.; Gras, M.; Lota, G.; Gniadek, M.; Romero, E.; Echegoyen, L.; Plonska-Brzezinska, M.E. Improvement of the Structural and Chemical Properties of Carbon Nano-onions for Electrocatalysis. *ChemNanoMat* **2017**, *3*, 583–590. [[CrossRef](#)]
49. Liu, D.; Ni, K.; Ye, J.; Xie, J.; Zhu, Y.; Song, L. Carbon Nanomaterials: Tailoring the Structure of Carbon Nanomaterials toward High-End Energy Applications. *Adv. Mater.* **2018**, *30*, 1870371. [[CrossRef](#)]
50. Zhang, C.; Shen, W.; Guo, K.; Xiong, M.; Zhang, J.; Lu, X. A Pentagonal Defect-Rich Metal-Free Carbon Electrocatalyst for Boosting Acidic O₂ Reduction to H₂O₂ Production. *J. Am. Chem. Soc.* **2023**, *145*, 11589–11598. [[CrossRef](#)]
51. Miller, J.R.; Simon, P. The Chalkboard: Fundamentals of Electrochemical Capacitor Design and Operation. *Electrochem. Soc. Interface* **2008**, *17*, 31–32. [[CrossRef](#)]
52. Simon, P.; Gogotsi, Y. Perspectives for Electrochemical Capacitors and Related Devices. *Nat. Mater.* **2020**, *19*, 1151–1163. [[CrossRef](#)] [[PubMed](#)]
53. Largeot, C.; Portet, C.; Chmiola, J.; Taberna, P.-L.; Gogotsi, Y.; Simon, P. Relation between the Ion Size and Pore Size for an Electric Double-Layer Capacitor. *J. Am. Chem. Soc.* **2008**, *130*, 2730–2731. [[CrossRef](#)]
54. Wu, X.; Yu, M.; Liu, J.; Li, S.; Zhang, X. Sp³-Defect and Pore Engineered Carbon Framework for High Energy Density Supercapacitors. *J. Power Sources* **2020**, *464*, 228203. [[CrossRef](#)]
55. Chen, J.; Han, Y.; Kong, X.; Deng, X.; Park, H.J.; Guo, Y.; Jin, S.; Qi, Z.; Lee, Z.; Qiao, Z.; et al. The Origin of Improved Electrical Double-Layer Capacitance by Inclusion of Topological Defects and Dopants in Graphene for Supercapacitors. *Angew. Chem. Int. Ed.* **2016**, *55*, 13822–13827. [[CrossRef](#)] [[PubMed](#)]
56. Jourdain, V.; Bichara, C. Current Understanding of the Growth of Carbon Nanotubes in Catalytic Chemical Vapour Deposition. *Carbon* **2013**, *58*, 2–39. [[CrossRef](#)]
57. Bacsá, R.R.; Laurent, C.; Peigney, A.; Bacsá, W.S.; Vaugien, T.; Rousset, A. High Specific Surface Area Carbon Nanotubes from Catalytic Chemical Vapor Deposition Process. *Chem. Phys. Lett.* **2000**, *323*, 566–571. [[CrossRef](#)]
58. Yamamoto, G.; Shirasu, K.; Nozaka, Y.; Sato, Y.; Takagi, T.; Hashida, T. Structure–Property Relationships in Thermally-Annealed Multi-Walled Carbon Nanotubes. *Carbon* **2014**, *66*, 219–226. [[CrossRef](#)]
59. Bom, D.; Andrews, R.; Jacques, D.; Anthony, J.; Chen, B.; Meier, M.S.; Selegue, J.P. Thermogravimetric Analysis of the Oxidation of Multiwalled Carbon Nanotubes: Evidence for the Role of Defect Sites in Carbon Nanotube Chemistry. *Nano Lett.* **2002**, *2*, 615–619. [[CrossRef](#)]

60. Xu, X.; Xu, C.; Liu, J.; Jin, R.; Luo, X.; Shu, C.; Chen, H.; Guo, C.; Xu, L.; Si, Y. The Synergistic Effect of “Soft-Hard Template” to in Situ Regulate Mass Transfer and Defective Sites of Doped-Carbon Nanostructures for Catalysis of Oxygen Reduction. *J. Alloys Compd.* **2023**, *939*, 168782. [CrossRef]
61. Benito, A.M.; Maniette, Y.; Muñoz, E.; Martínez, M.T. Carbon Nanotubes Production by Catalytic Pyrolysis of Benzene. *Carbon* **1998**, *36*, 681–683. [CrossRef]
62. Lin, W.; Moon, K.-S.; Zhang, S.; Ding, Y.; Shang, J.; Chen, M.; Wong, C. Microwave Makes Carbon Nanotubes Less Defective. *ACS Nano* **2010**, *4*, 1716–1722. [CrossRef] [PubMed]
63. Vázquez, E.; Prato, M. Carbon Nanotubes and Microwaves: Interactions, Responses, and Applications. *ACS Nano* **2009**, *3*, 3819–3824. [CrossRef] [PubMed]
64. Mubarak, N.M.; Sahu, J.N.; Abdullah, E.C.; Jayakumar, N.S.; Ganesan, P. Single Stage Production of Carbon Nanotubes Using Microwave Technology. *Diam. Relat. Mater.* **2014**, *48*, 52–59. [CrossRef]
65. Hong, E.H.; Lee, K.-H.; Oh, S.H.; Park, C.-G. Synthesis of Carbon Nanotubes Using Microwave Radiation. *Adv. Funct. Mater.* **2003**, *13*, 961–966. [CrossRef]
66. Bulusheva, L.G.; Arkhipov, V.E.; Popov, K.M.; Sysoev, V.I.; Makarova, A.A.; Okotrub, A.V. Electronic Structure of Nitrogen- and Phosphorus-Doped Graphenes Grown by Chemical Vapor Deposition Method. *Materials* **2020**, *13*, 1173. [CrossRef] [PubMed]
67. Masikhwa, T.M.; Madito, M.J.; Bello, A.; Lekitima, J.; Manyala, N. Microwave-Assisted Synthesis of Cobalt Sulphide Nanoparticle Clusters on Activated Graphene Foam for Electrochemical Supercapacitors. *RSC Adv.* **2017**, *7*, 20231–20240. [CrossRef]
68. Yan, K.; Sun, X.; Ying, S.; Cheng, W.; Deng, Y.; Ma, Z.; Zhao, Y.; Wang, X.; Pan, L.; Shi, Y. Ultrafast Microwave Synthesis of Rambutan-like CMK-3/Carbon Nanotubes Nanocomposites for High-Performance Supercapacitor Electrode Materials. *Sci. Rep.* **2020**, *10*, 6227. [CrossRef]
69. Lin, Y.; Zhu, Y.; Zhang, B.; Kim, Y.A.; Endo, M.; Su, D.S. Boron-Doped Onion-like Carbon with Enriched Substitutional Boron: The Relationship between Electronic Properties and Catalytic Performance. *J. Mater. Chem. A* **2015**, *3*, 21805–21814. [CrossRef]
70. Plonska-Brzezinska, M.E.; Dubis, A.T.; Lapinski, A.; Villalta-Cerdas, A.; Echegoyen, L. Electrochemical Properties of Oxidized Carbon Nano-Onions: DRIFTS-FTIR and Raman Spectroscopic Analyses. *ChemPhysChem* **2011**, *12*, 2659–2668. [CrossRef]
71. Xiao, B.; Boudou, J.P.; Thomas, K.M. Reactions of Nitrogen and Oxygen Surface Groups in Nanoporous Carbons under Inert and Reducing Atmospheres. *Langmuir* **2005**, *21*, 3400–3409. [CrossRef] [PubMed]
72. Datsyuk, V.; Kalyva, M.; Papagelis, K.; Parthenios, J.; Tasis, D.; Siokou, A.; Kallitsis, I.; Galiotis, C. Chemical Oxidation of Multiwalled Carbon Nanotubes. *Carbon* **2008**, *46*, 833–840. [CrossRef]
73. Plonska-Brzezinska, M.E.; Lapinski, A.; Wilczewska, A.Z.; Dubis, A.T.; Villalta-Cerdas, A.; Winkler, K.; Echegoyen, L. The Synthesis and Characterization of Carbon Nano-Onions Produced by Solution Ozonolysis. *Carbon* **2011**, *49*, 5079–5089. [CrossRef]
74. Yang, D.-Q.; Sacher, E. Strongly Enhanced Interaction between Evaporated Pt Nanoparticles and Functionalized Multiwalled Carbon Nanotubes via Plasma Surface Modifications: Effects of Physical and Chemical Defects. *J. Phys. Chem. C* **2008**, *112*, 4075–4082. [CrossRef]
75. Zschoerper, N.P.; Katzenmaier, V.; Vohrer, U.; Haupt, M.; Oehr, C.; Hirth, T. Analytical Investigation of the Composition of Plasma-Induced Functional Groups on Carbon Nanotube Sheets. *Carbon* **2009**, *47*, 2174–2185. [CrossRef]
76. Liu, J.; Zubiri, M.R.I.; Vigolo, B.; Dossot, M.; Fort, Y.; Ehrhardt, J.-J.; McRae, E. Efficient Microwave-Assisted Radical Functionalization of Single-Wall Carbon Nanotubes. *Carbon* **2007**, *45*, 885–891. [CrossRef]
77. Kuo, C.-Y. Comparison with As-Grown and Microwave Modified Carbon Nanotubes to Removal Aqueous Bisphenol A. *Desalination* **2009**, *249*, 976–982. [CrossRef]
78. Deng, D.; Yu, L.; Pan, X.; Wang, S.; Chen, X.; Hu, P.; Sun, L.; Bao, X. Size Effect of Graphene on Electrocatalytic Activation of Oxygen. *Chem. Commun.* **2011**, *47*, 10016. [CrossRef]
79. Liu, D.; Ni, K.; Ye, J.; Xie, J.; Zhu, Y.; Song, L. Tailoring the Structure of Carbon Nanomaterials toward High-End Energy Applications. *Adv. Mater.* **2018**, *30*, 1802104. [CrossRef]
80. Kotakoski, J.; Krasheninnikov, A.V.; Kaiser, U.; Meyer, J.C. From Point Defects in Graphene to Two-Dimensional Amorphous Carbon. *Phys. Rev. Lett.* **2011**, *106*, 105505. [CrossRef]
81. Yang, H.B.; Miao, J.; Hung, S.-F.; Chen, J.; Tao, H.B.; Wang, X.; Zhang, L.; Chen, R.; Gao, J.; Chen, H.M.; et al. Identification of Catalytic Sites for Oxygen Reduction and Oxygen Evolution in N-Doped Graphene Materials: Development of Highly Efficient Metal-Free Bifunctional Electrocatalyst. *Sci. Adv.* **2016**, *2*, e1501122. [CrossRef] [PubMed]
82. Jia, Y.; Chen, J.; Yao, X. Defect Electrocatalytic Mechanism: Concept, Topological Structure and Perspective. *Mater. Chem. Front.* **2018**, *2*, 1250–1268. [CrossRef]
83. Dresselhaus, M.S.; Jorio, A.; Souza Filho, A.G.; Saito, R. Defect characterization in graphene and carbon nanotubes using Raman spectroscopy. *Phil. Trans. R. Soc. A* **2010**, *368*, 5355–5377. [CrossRef] [PubMed]
84. Trevethan, T.; Latham, C.D.; Heggie, M.I.; Briddon, P.R.; Rayson, M.J. Vacancy Diffusion and Coalescence in Graphene Directed by Defect Strain Fields. *Nanoscale* **2014**, *6*, 2978–2986. [CrossRef] [PubMed]
85. Li, Z.; Peng, H.; Liu, R.; Mo, Y.; Cao, B.; Lai, W.; Li, X.; Pan, L.; Chen, Y. Quantitative Assessment of Basal-, Edge- and Defect-Surfaces of Carbonaceous Materials and Their Influence on Electric Double-Layer Capacitance. *J. Power Sources* **2020**, *457*, 228022. [CrossRef]
86. Wang, Y.; Zhu, Y.; Wu, H. Formation and Topological Structure of Three-Dimensional Disordered Graphene Networks. *Phys. Chem. Chem. Phys.* **2021**, *23*, 10290–10302. [CrossRef] [PubMed]

87. Ma, J.; Alfè, D.; Michaelides, A.; Wang, E. Stone-Wales Defects in Graphene and Other Planar sp^2 -Bonded Materials. *Phys. Rev. B* **2009**, *80*, 033407. [[CrossRef](#)]
88. Akhunova, A.K.; Galiakhmetova, L.K.; Baimova, J.A. The Effects of Dislocation Dipoles on the Failure Strength of Wrinkled Graphene from Atomistic Simulation. *Appl. Sci.* **2022**, *13*, 9. [[CrossRef](#)]
89. Zhao, S.; Guo, Z.; Yang, J.; Wang, C.; Sun, B.; Wang, G. Nanoengineering of Advanced Carbon Materials for Sodium-Ion Batteries. *Small* **2021**, *17*, 2007431. [[CrossRef](#)]
90. Pastor, E.; Sachs, M.; Selim, S.; Durrant, J.R.; Bakulin, A.A.; Walsh, A. Electronic Defects in Metal Oxide Photocatalysts. *Nat. Rev. Mater.* **2022**, *7*, 503–521. [[CrossRef](#)]
91. Okuyama, Y.; Kurita, N.; Fukatsu, N. Defect Structure of Alumina-Rich Nonstoichiometric Magnesium Aluminate Spinel. *Solid State Ion.* **2006**, *177*, 59–64. [[CrossRef](#)]
92. Frauenheim, T.; Blaudeck, P.; Stephan, U.; Jungnickel, G. Atomic Structure and Physical Properties of Amorphous Carbon and Its Hydrogenated Analogs. *Phys. Rev. B* **1993**, *48*, 4823–4834. [[CrossRef](#)] [[PubMed](#)]
93. Cho, N.-H.; Krishnan, K.M.; Veirs, D.K.; Rubin, M.D.; Hopper, C.B.; Bhushan, B.; Bogy, D.B. Chemical Structure and Physical Properties of Diamond-like Amorphous Carbon Films Prepared by Magnetron Sputtering. *J. Mater. Res.* **1990**, *5*, 2543–2554. [[CrossRef](#)]
94. Mounier, E.; Bertin, F.; Adamik, M.; Pauleau, Y.; Barna, P.B. Effect of the Substrate Temperature on the Physical Characteristics of Amorphous Carbon Films Deposited by d.c. Magnetron Sputtering. *Diam. Relat. Mater.* **1996**, *5*, 1509–1515. [[CrossRef](#)]
95. Miller, D. *Building a Project Work Breakdown Structure: Visualizing Objectives, Deliverables, Activities, and Schedules*; ESI International Project Management Series; Auerbach Publications: Boca Raton, FL, USA, 2008; Volume 20085940, ISBN 978-1-4200-6969-3.
96. Bandaru, P.R.; Yamada, H.; Narayanan, R.; Hofer, M. Charge Transfer and Storage in Nanostructures. *Mater. Sci. Eng. R Rep.* **2015**, *96*, 1–69. [[CrossRef](#)]
97. Bagge-Hansen, M.; Bastea, S.; Hammons, J.A.; Nielsen, M.H.; Lauderbach, L.M.; Hodgkin, R.L.; Pagoria, P.; May, C.; Aloni, S.; Jones, A.; et al. Detonation Synthesis of Carbon Nano-Onions via Liquid Carbon Condensation. *Nat. Commun.* **2019**, *10*, 3819. [[CrossRef](#)] [[PubMed](#)]
98. Moussa, G.; Matei Ghimbeu, C.; Taberna, P.-L.; Simon, P.; Vix-Guterl, C. Relationship between the Carbon Nano-Onions (CNOs) Surface Chemistry/Defects and Their Capacitance in Aqueous and Organic Electrolytes. *Carbon* **2016**, *105*, 628–637. [[CrossRef](#)]
99. Deng, J.-H.; Cheng, L.; Wang, F.-J.; Yu, B.; Li, G.-Z.; Li, D.-J.; Cheng, G.-A. Ultralow Field Emission from Thinned, Open-Ended, and Defected Carbon Nanotubes by Using Microwave Hydrogen Plasma Processing. *Appl. Surf. Sci.* **2015**, *324*, 293–299. [[CrossRef](#)]
100. Ferrari, A.C.; Meyer, J.C.; Scardaci, V.; Casiraghi, C.; Lazzeri, M.; Mauri, F.; Piscanec, S.; Jiang, D.; Novoselov, K.S.; Roth, S.; et al. Raman Spectrum of Graphene and Graphene Layers. *Phys. Rev. Lett.* **2006**, *97*, 187401. [[CrossRef](#)]
101. Tuinstra, F.; Koenig, J.L. Raman Spectrum of Graphite. *J. Chem. Phys.* **1970**, *53*, 1126–1130. [[CrossRef](#)]
102. Fowler, R.H.; Nordheim, L. Electron Emission in Intense Electric Fields. *Proc. R. Soc. Lond. Ser. Contain. Pap. Math. Phys. Character* **1928**, *119*, 173–181. [[CrossRef](#)]
103. Borgohain, R.; Li, J.; Selegue, J.P.; Cheng, Y.-T. Electrochemical Study of Functionalized Carbon Nano-Onions for High-Performance Supercapacitor Electrodes. *J. Phys. Chem. C* **2012**, *116*, 15068–15075. [[CrossRef](#)]
104. Portet, C.; Yushin, G.; Gogotsi, Y. Electrochemical Performance of Carbon Onions, Nanodiamonds, Carbon Black and Multiwalled Nanotubes in Electrical Double Layer Capacitors. *Carbon* **2007**, *45*, 2511–2518. [[CrossRef](#)]
105. Liu, X.; Antonietti, M. Molten Salt Activation for Synthesis of Porous Carbon Nanostructures and Carbon Sheets. *Carbon* **2014**, *69*, 460–466. [[CrossRef](#)]
106. Wang, J.-G.; Liu, H.; Zhang, X.; Li, X.; Liu, X.; Kang, F. Green Synthesis of Hierarchically Porous Carbon Nanotubes as Advanced Materials for High-Efficient Energy Storage. *Small* **2018**, *14*, 1703950. [[CrossRef](#)] [[PubMed](#)]
107. Wang, P.; Ye, H.; Yin, Y.; Chen, H.; Bian, Y.; Wang, Z.; Cao, F.; Guo, Y. Fungi-Enabled Synthesis of Ultrahigh-Surface-Area Porous Carbon. *Adv. Mater.* **2019**, *31*, 1805134. [[CrossRef](#)] [[PubMed](#)]
108. Pech, D.; Brunet, M.; Durou, H.; Huang, P.; Mochalin, V.; Gogotsi, Y.; Taberna, P.-L.; Simon, P. Ultrahigh-Power Micrometre-Sized Supercapacitors Based on Onion-like Carbon. *Nat. Nanotechnol.* **2010**, *5*, 651–654. [[CrossRef](#)]
109. Zeiger, M.; Jäckel, N.; Aslan, M.; Weingarth, D.; Presser, V. Understanding Structure and Porosity of Nanodiamond-Derived Carbon Onions. *Carbon* **2015**, *84*, 584–598. [[CrossRef](#)]
110. An, Y.; Li, C.; Sun, X.; Wang, K.; Su, F.; Liu, F.; Zhang, X.; Ma, Y. Deoxygenated Porous Carbon with Highly Stable Electrochemical Reaction Interface for Practical High-Performance Lithium-Ion Capacitors. *J. Phys. Appl. Phys.* **2022**, *55*, 045501. [[CrossRef](#)]
111. Wang, C.; Chi, M.; Wang, G.; van der Vliet, D.; Li, D.; More, K.; Wang, H.-H.; Schlueter, J.A.; Markovic, N.M.; Stamenkovic, V.R. Correlation between Surface Chemistry and Electrocatalytic Properties of Monodisperse PtxNi1-x Nanoparticles. *Adv. Funct. Mater.* **2011**, *21*, 147–152. [[CrossRef](#)]
112. Trasatti, S. Oxide/Aqueous Solution Interfaces, Interplay of Surface Chemistry and Electrocatalysis. *Mater. Chem. Phys.* **1987**, *16*, 157–174. [[CrossRef](#)]
113. Chen, D.; Zou, Y.; Wang, S. Surface Chemical-Functionalization of Ultrathin Two-Dimensional Nanomaterials for Electrocatalysis. *Mater. Today Energy* **2019**, *12*, 250–268. [[CrossRef](#)]
114. Chatterjee, K.; Ashokkumar, M.; Gullapalli, H.; Gong, Y.; Vajtai, R.; Thanikaivelan, P.; Ajayan, P.M. Nitrogen-Rich Carbon Nano-Onions for Oxygen Reduction Reaction. *Carbon* **2018**, *130*, 645–651. [[CrossRef](#)]

115. Jain, D.; Mamtani, K.; Gustin, V.; Gunduz, S.; Celik, G.; Waluyo, I.; Hunt, A.; Co, A.C.; Ozkan, U.S. Enhancement in Oxygen Reduction Reaction Activity of Nitrogen-Doped Carbon Nanostructures in Acidic Media through Chloride-Ion Exposure. *ChemElectroChem* **2018**, *5*, 1966–1975. [[CrossRef](#)]
116. Cabioch, T.; Rivière, J.P.; Jaouen, M.; Delafond, J.; Denanot, M.F. Fullerene Onion Formation by Carbon-Ion Implantation into Copper. *Synth. Met.* **1996**, *77*, 253–256. [[CrossRef](#)]
117. Butsyk, O.; Olejnik, P.; Romero, E.; Plonska-Brzezinska, M.E. Postsynthetic Treatment of Carbon Nano-Onions: Surface Modification by Heteroatoms to Enhance Their Capacitive and Electrocatalytic Properties. *Carbon* **2019**, *147*, 90–104. [[CrossRef](#)]
118. Domga; Karnan, M.; Oladoyinbo, F.; Noumi, G.B.; Tchatchueng, J.B.; Sieliechi, M.J.; Sathish, M.; Pattanayak, D.K. A Simple, Economical One-Pot Microwave Assisted Synthesis of Nitrogen and Sulfur Co-Doped Graphene for High Energy Supercapacitors. *Electrochim. Acta* **2020**, *341*, 135999. [[CrossRef](#)]
119. Savilov, S.V.; Arkhipova, E.A.; Ivanov, A.S.; Maslakov, K.I.; Shen, Z.; Aldoshin, S.M.; Lunin, V.V. Pyrolytic Synthesis and Characterization of N-Doped Carbon Nanoflakes for Electrochemical Applications. *Mater. Res. Bull.* **2015**, *69*, 7–12. [[CrossRef](#)]
120. Szymanski, G.S.; Suzuki, Y.; Ohba, T.; Sulikowski, B.; Góra-Marek, K.; Tarach, K.A.; Koter, S.; Kowalczyk, P.; Ilnicka, A.; Zięba, M.; et al. Linking the Defective Structure of Boron-Doped Carbon Nano-Onions with Their Catalytic Properties: Experimental and Theoretical Studies. *ACS Appl. Mater. Interfaces* **2021**, *13*, 51628–51642. [[CrossRef](#)]
121. Yu, H.; Jin, Y.; Peng, F.; Wang, H.; Yang, J. Kinetically Controlled Side-Wall Functionalization of Carbon Nanotubes by Nitric Acid Oxidation. *J. Phys. Chem. C* **2008**, *112*, 6758–6763. [[CrossRef](#)]
122. Zhang, J.; Zou, H.; Qing, Q.; Yang, Y.; Li, Q.; Liu, Z.; Guo, X.; Du, Z. Effect of Chemical Oxidation on the Structure of Single-Walled Carbon Nanotubes. *J. Phys. Chem. B* **2003**, *107*, 3712–3718. [[CrossRef](#)]
123. Xing, Y.; Li, L.; Chusuei, C.C.; Hull, R.V. Sonochemical Oxidation of Multiwalled Carbon Nanotubes. *Langmuir* **2005**, *21*, 4185–4190. [[CrossRef](#)] [[PubMed](#)]
124. Martín, O.; Gutierrez, H.R.; Maroto-Valiente, A.; Terrones, M.; Blanco, T.; Baselga, J. An Efficient Method for the Carboxylation of Few-Wall Carbon Nanotubes with Little Damage to Their Sidewalls. *Mater. Chem. Phys.* **2013**, *140*, 499–507. [[CrossRef](#)]
125. Wu, H.; Li, Z.; Ji, D.; Liu, Y.; Li, L.; Yuan, D.; Zhang, Z.; Ren, J.; Lefler, M.; Wang, B.; et al. One-Pot Synthesis of Nanostructured Carbon Materials from Carbon Dioxide via Electrolysis in Molten Carbonate Salts. *Carbon* **2016**, *106*, 208–217. [[CrossRef](#)]
126. Gonzalez-Aguilar, J.; Moreno, M.; Fulcheri, L. Carbon Nanostructures Production by Gas-Phase Plasma Processes at Atmospheric Pressure. *J. Phys. Appl. Phys.* **2007**, *40*, 2361–2374. [[CrossRef](#)]
127. Wang, X.; Li, N.; Webb, J.A.; Pfefferle, L.D.; Haller, G.L. Effect of Surface Oxygen Containing Groups on the Catalytic Activity of Multi-Walled Carbon Nanotube Supported Pt Catalyst. *Appl. Catal. B Environ.* **2010**, *101*, 21–30. [[CrossRef](#)]
128. Liu, Z.-Q.; Ma, J.; Cui, Y.-H.; Zhang, B.-P. Effect of Ozonation Pretreatment on the Surface Properties and Catalytic Activity of Multi-Walled Carbon Nanotube. *Appl. Catal. B Environ.* **2009**, *92*, 301–306. [[CrossRef](#)]
129. Fedorovskaya, E.O.; Bulusheva, L.G.; Kurenaya, A.G.; Asanov, I.P.; Okotrub, A.V. Effect of Oxidative Treatment on the Electrochemical Properties of Aligned Multi-Walled Carbon Nanotubes. *Russ. J. Electrochem.* **2016**, *52*, 441–448. [[CrossRef](#)]
130. Frackowiak, E.; Beguin, F. Electrochemical Storage of Energy in Carbon Nanotubes and Nanostructured Carbons. *Carbon* **2002**, *40*, 1775–1787. [[CrossRef](#)]
131. Pawelski, D.; Delgado, O.F.; Wilczewska, A.Z.; Strawa, J.W.; Plonska-Brzezinska, M.E. Nanostructured Carbon Catalyst for Amide Coupling Reactions under Microwave Heating in the Absence of a Solvent. *ACS Appl. Nano Mater.* **2022**, *5*, 16376–16387. [[CrossRef](#)]
132. Lin, Y.; Wu, S.; Shi, W.; Zhang, B.; Wang, J.; Kim, Y.A.; Endo, M.; Su, D.S. Efficient and Highly Selective Boron-Doped Carbon Materials-Catalyzed Reduction of Nitroarenes. *Chem. Commun.* **2015**, *51*, 13086–13089. [[CrossRef](#)] [[PubMed](#)]
133. Dong, Y.; Zhang, S.; Du, X.; Hong, S.; Zhao, S.; Chen, Y.; Chen, X.; Song, H. Boosting the Electrical Double-Layer Capacitance of Graphene by Self-Doped Defects through Ball-Milling. *Adv. Funct. Mater.* **2019**, *29*, 1901127. [[CrossRef](#)]
134. Szymański, G.S.; Wiśniewski, M.; Olejnik, P.; Koter, S.; Castro, E.; Echegoyen, L.; Terzyk, A.P.; Plonska-Brzezinska, M.E. Correlation between the Catalytic and Electrocatalytic Properties of Nitrogen-Doped Carbon Nanooxions and the Polarity of the Carbon Surface: Experimental and Theoretical Investigations. *Carbon* **2019**, *151*, 120–129. [[CrossRef](#)]
135. Kumar, R.; Sahoo, S.; Joanni, E.; Singh, R.K.; Maegawa, K.; Tan, W.K.; Kawamura, G.; Kar, K.K.; Matsuda, A. Heteroatom Doped Graphene Engineering for Energy Storage and Conversion. *Mater. Today* **2020**, *39*, 47–65. [[CrossRef](#)]
136. Basivi, P.K.; Pasupuleti, K.S.; Gelija, D.; Kim, M.-D.; Pasupuleti, V.R.; Kim, C.W. UV-Light-Enhanced Room Temperature NO₂ Gas-Sensing Performances Based on Sulfur-Doped Graphitic Carbon Nitride Nanoflakes. *N. J. Chem.* **2022**, *46*, 19254–19262. [[CrossRef](#)]
137. Fortunato, G.V.; Kronka, M.S.; Cardoso, E.S.F.; dos Santos, A.J.; Roveda, A.C.; Lima, F.H.B.; Ledendecker, M.; Maia, G.; Lanza, M.R.V. A Comprehensive Comparison of Oxygen and Nitrogen Functionalities in Carbon and Their Implications for the Oxygen Reduction Reaction. *J. Catal.* **2022**, *413*, 1034–1047. [[CrossRef](#)]
138. Zheng, Y.; Jiao, Y.; Li, L.H.; Xing, T.; Chen, Y.; Jaroniec, M.; Qiao, S.Z. Toward Design of Synergistically Active Carbon-Based Catalysts for Electrocatalytic Hydrogen Evolution. *ACS Nano* **2014**, *8*, 5290–5296. [[CrossRef](#)]
139. Guo, D.; Shibuya, R.; Akiba, C.; Saji, S.; Kondo, T.; Nakamura, J. Active Sites of Nitrogen-Doped Carbon Materials for Oxygen Reduction Reaction Clarified Using Model Catalysts. *Science* **2016**, *351*, 361–365. [[CrossRef](#)]
140. Zhao, Z.; Li, M.; Zhang, L.; Dai, L.; Xia, Z. Design Principles for Heteroatom-Doped Carbon Nanomaterials as Highly Efficient Catalysts for Fuel Cells and Metal-Air Batteries. *Adv. Mater.* **2015**, *27*, 6834–6840. [[CrossRef](#)]

141. Ortiz-Medina, J.; Wang, Z.; Cruz-Silva, R.; Morelos-Gomez, A.; Wang, F.; Yao, X.; Terrones, M.; Endo, M. Defect Engineering and Surface Functionalization of Nanocarbons for Metal-Free Catalysis. *Adv. Mater.* **2019**, *31*, 1805717. [[CrossRef](#)]
142. Zhao, Y.; Yang, L.; Chen, S.; Wang, X.; Ma, Y.; Wu, Q.; Jiang, Y.; Qian, W.; Hu, Z. Can Boron and Nitrogen Co-Doping Improve Oxygen Reduction Reaction Activity of Carbon Nanotubes? *J. Am. Chem. Soc.* **2013**, *135*, 1201–1204. [[CrossRef](#)]
143. Zheng, Y.; Jiao, Y.; Ge, L.; Jaroniec, M.; Qiao, S.Z. Two-Step Boron and Nitrogen Doping in Graphene for Enhanced Synergistic Catalysis. *Angew. Chem. Int. Ed.* **2013**, *52*, 3110–3116. [[CrossRef](#)]
144. Tang, C.; Zhang, Q. Nanocarbon for Oxygen Reduction Electrocatalysis: Dopants, Edges, and Defects. *Adv. Mater.* **2017**, *29*, 1604103. [[CrossRef](#)] [[PubMed](#)]
145. Fedoseeva, Y.V.; Lapteva, L.L.; Makarova, A.A.; Bulusheva, L.G.; Okotrub, A.V. Charge Polarization in Partially Lithiated Single-Walled Carbon Nanotubes. *Phys. Chem. Chem. Phys.* **2018**, *20*, 22592–22599. [[CrossRef](#)] [[PubMed](#)]
146. Bulusheva, L.G.; Okotrub, A.V.; Kuznetsov, V.L.; Vyalikh, D.V. Soft X-Ray Spectroscopy and Quantum Chemistry Characterization of Defects in Onion-like Carbon Produced by Nanodiamond Annealing. *Diam. Relat. Mater.* **2007**, *16*, 1222–1226. [[CrossRef](#)]
147. Fedoseeva, Y.V.; Okotrub, A.V.; Koroteev, V.O.; Borzdov, Y.M.; Palyanov, Y.N.; Shubin, Y.V.; Maksimovskiy, E.A.; Makarova, A.A.; Münchgesang, W.; Bulusheva, L.G.; et al. Graphitization of ¹³C Enriched Fine-Grained Graphitic Material under High-Pressure Annealing. *Carbon* **2019**, *141*, 323–330. [[CrossRef](#)]
148. Pacilé, D.; Meyer, J.C.; Fraile Rodríguez, A.; Papagno, M.; Gómez-Navarro, C.; Sundaram, R.S.; Burghard, M.; Kern, K.; Carbone, C.; Kaiser, U. Electronic Properties and Atomic Structure of Graphene Oxide Membranes. *Carbon* **2011**, *49*, 966–972. [[CrossRef](#)]
149. Hua, W.; Gao, B.; Li, S.; Ågren, H.; Luo, Y. X-Ray Absorption Spectra of Graphene from First-Principles Simulations. *Phys. Rev. B* **2010**, *82*, 155433. [[CrossRef](#)]
150. Isacsson, A.; Cummings, A.W.; Colombo, L.; Colombo, L.; Kinaret, J.M.; Roche, S. Scaling Properties of Polycrystalline Graphene: A Review. *2D Mater.* **2016**, *4*, 012002. [[CrossRef](#)]
151. Duan, Z.; Han, G.; Huo, H.; Lin, Z.; Ge, L.; Du, C.; Gao, Y.; Yin, G. Monovacancy Coupled Pyridinic N Site Enables Surging Oxygen Reduction Activity of Metal-Free CN_x Catalyst. *ACS Sustain. Chem. Eng.* **2021**, *9*, 1264–1271. [[CrossRef](#)]
152. Yang, L.; Jiang, S.; Zhao, Y.; Zhu, L.; Chen, S.; Wang, X.; Wu, Q.; Ma, J.; Ma, Y.; Hu, Z. Boron-Doped Carbon Nanotubes as Metal-Free Electrocatalysts for the Oxygen Reduction Reaction. *Angew. Chem. Int. Ed.* **2011**, *50*, 7132–7135. [[CrossRef](#)] [[PubMed](#)]
153. Sheng, Z.-H.; Gao, H.-L.; Bao, W.-J.; Wang, F.-B.; Xia, X.-H. Synthesis of Boron Doped Graphene for Oxygen Reduction Reaction in Fuel Cells. *J. Mater. Chem.* **2012**, *22*, 390–395. [[CrossRef](#)]
154. Pourazadi, E.; Haque, E.; Zhang, W.; Harris, A.T.; Minett, A.I. Synergistically Enhanced Electrochemical (ORR) Activity of Graphene Oxide Using Boronic Acid as an Interlayer Spacer. *Chem. Commun.* **2013**, *49*, 11068. [[CrossRef](#)] [[PubMed](#)]
155. Shaikh, A.; Singh, B.K.; Mohapatra, D.; Parida, S. Nitrogen-Doped Carbon Nano-Onions as a Metal-Free Electrocatalyst. *Electrocatalysis* **2019**, *10*, 222–231. [[CrossRef](#)]
156. Jia, Y.; Zhang, L.; Du, A.; Gao, G.; Chen, J.; Yan, X.; Brown, C.L.; Yao, X. Defect Graphene as a Trifunctional Catalyst for Electrochemical Reactions. *Adv. Mater.* **2016**, *28*, 9532–9538. [[CrossRef](#)]
157. Sa, Y.J.; Park, C.; Jeong, H.Y.; Park, S.-H.; Lee, Z.; Kim, K.T.; Park, G.-G.; Joo, S.H. Carbon Nanotubes/Heteroatom-Doped Carbon Core-Sheath Nanostructures as Highly Active, Metal-Free Oxygen Reduction Electrocatalysts for Alkaline Fuel Cells. *Angew. Chem. Int. Ed.* **2014**, *53*, 4102–4106. [[CrossRef](#)]
158. Victoria Tafoya, J.P.; Doszczeczko, S.; Titirici, M.M.; Jorge Sobrido, A.B. Enhancement of the Electrocatalytic Activity for the Oxygen Reduction Reaction of Boron-Doped Reduced Graphene Oxide via Ultrasonic Treatment. *Int. J. Hydrog. Energy* **2022**, *47*, 5462–5473. [[CrossRef](#)]
159. Sedelnikova, O.V.; Fedoseeva, Y.V.; Romanenko, A.I.; Gusel'nikov, A.V.; Vilkov, O.Y.; Maksimovskiy, E.A.; Bychanok, D.S.; Kuzhir, P.P.; Bulusheva, L.G.; Okotrub, A.V. Effect of Boron and Nitrogen Additives on Structure and Transport Properties of Arc-Produced Carbon. *Carbon* **2019**, *143*, 660–668. [[CrossRef](#)]
160. Lai, Q.; Wei, K.; Tang, Z.; Liu, X.; Zheng, J.; Liang, Y. Edge Reconfiguration of N, P-Codoped Carbon Boosts Oxygen Reduction Electrocatalysis. *J. Mater. Sci.* **2021**, *56*, 19577–19588. [[CrossRef](#)]
161. Camisasca, A.; Sacco, A.; Brescia, R.; Giordani, S. Boron/Nitrogen-Codoped Carbon Nano-Onion Electrocatalysts for the Oxygen Reduction Reaction. *ACS Appl. Nano Mater.* **2018**, *1*, 5763–5773. [[CrossRef](#)]
162. Pinto, H.; Markevich, A. Electronic and Electrochemical Doping of Graphene by Surface Adsorbates. *Beilstein J. Nanotechnol.* **2014**, *5*, 1842–1848. [[CrossRef](#)] [[PubMed](#)]
163. Kepaptsoglou, D.; Hardcastle, T.P.; Seabourne, C.R.; Bangert, U.; Zan, R.; Amani, J.A.; Hofsäss, H.; Nicholls, R.J.; Brydson, R.M.D.; Scott, A.J.; et al. Electronic Structure Modification of Ion Implanted Graphene: The Spectroscopic Signatures of p- and n-Type Doping. *ACS Nano* **2015**, *9*, 11398–11407. [[CrossRef](#)] [[PubMed](#)]
164. Chauhan, S.S.; Srivastava, P.; Shrivastava, A.K. Electronic and Transport Properties of Boron and Nitrogen Doped Graphene Nanoribbons: An Ab Initio Approach. *Appl. Nanosci.* **2014**, *4*, 461–467. [[CrossRef](#)]
165. Sikeyi, L.L.; Ntuli, T.D.; Mongwe, T.H.; Maxakato, N.W.; Carleschi, E.; Doyle, B.P.; Coville, N.J.; Maubane-Nkadimeng, M.S. Microwave Assisted Synthesis of Nitrogen Doped and Oxygen Functionalized Carbon Nano Onions Supported Palladium Nanoparticles as Hybrid Anodic Electrocatalysts for Direct Alkaline Ethanol Fuel Cells. *Int. J. Hydrog. Energy* **2021**, *46*, 10862–10875. [[CrossRef](#)]
166. Kumar, R.; Sahoo, S.; Joanni, E.; Singh, R.K.; Kar, K.K. Microwave as a Tool for Synthesis of Carbon-Based Electrodes for Energy Storage. *ACS Appl. Mater. Interfaces* **2022**, *14*, 20306–20325. [[CrossRef](#)] [[PubMed](#)]

167. Schwenke, A.M.; Hoepfner, S.; Schubert, U.S. Synthesis and Modification of Carbon Nanomaterials Utilizing Microwave Heating. *Adv. Mater.* **2015**, *27*, 4113–4141. [[CrossRef](#)]
168. Kim, T.; Lee, J.; Lee, K.-H. Microwave Heating of Carbon-Based Solid Materials. *Carbon Lett.* **2014**, *15*, 15–24. [[CrossRef](#)]
169. Menéndez, J.A.; Arenillas, A.; Fidalgo, B.; Fernández, Y.; Zubizarreta, L.; Calvo, E.G.; Bermúdez, J.M. Microwave Heating Processes Involving Carbon Materials. *Fuel Process. Technol.* **2010**, *91*, 1–8. [[CrossRef](#)]
170. Umrao, S.; Gupta, T.K.; Kumar, S.; Singh, V.K.; Sultania, M.K.; Jung, J.H.; Oh, I.-K.; Srivastava, A. Microwave-Assisted Synthesis of Boron and Nitrogen Co-Doped Reduced Graphene Oxide for the Protection of Electromagnetic Radiation in Ku-Band. *ACS Appl. Mater. Interfaces* **2015**, *7*, 19831–19842. [[CrossRef](#)]
171. Liu, Z.; Zhang, L.; Poyraz, S.; Smith, J.; Kushvaha, V.; Tippur, H.; Zhang, X. An Ultrafast Microwave Approach towards Multi-Component and Multi-Dimensional Nanomaterials. *RSC Adv.* **2014**, *4*, 9308. [[CrossRef](#)]
172. Slocombe, D.; Porch, A.; Bustarret, E.; Williams, O.A. Microwave Properties of Nanodiamond Particles. *Appl. Phys. Lett.* **2013**, *102*, 244102. [[CrossRef](#)]
173. Chen, X.; Tian, X.; Zhou, Z.; Jiang, M.; Lu, J.; Wang, Y.; Wang, L. Effective Improvement in Microwave Absorption by Uniform Dispersion of Nanodiamond in Polyaniline through in-Situ Polymerization. *Appl. Phys. Lett.* **2015**, *106*, 233103. [[CrossRef](#)]
174. Yoon, B.-J.; Hong, E.H.; Jee, S.E.; Yoon, D.-M.; Shim, D.-S.; Son, G.-Y.; Lee, Y.J.; Lee, K.-H.; Kim, H.S.; Park, C.G. Fabrication of Flexible Carbon Nanotube Field Emitter Arrays by Direct Microwave Irradiation on Organic Polymer Substrate. *J. Am. Chem. Soc.* **2005**, *127*, 8234–8235. [[CrossRef](#)] [[PubMed](#)]
175. Ma, Z.; Yu, J.; Dai, S. Preparation of Inorganic Materials Using Ionic Liquids. *Adv. Mater.* **2010**, *22*, 261–285. [[CrossRef](#)]
176. Zhao, H.; Sun, C.; Jin, Z.; Wang, D.-W.; Yan, X.; Chen, Z.; Zhu, G.; Yao, X. Carbon for the Oxygen Reduction Reaction: A Defect Mechanism. *J. Mater. Chem. A* **2015**, *3*, 11736–11739. [[CrossRef](#)]
177. Pentsak, E.O.; Gordeev, E.G.; Ananikov, V.P. Noninnocent Nature of Carbon Support in Metal/Carbon Catalysts: Etching/Pitting vs Nanotube Growth under Microwave Irradiation. *ACS Catal.* **2014**, *4*, 3806–3814. [[CrossRef](#)]
178. Bajpai, R.; Wagner, H.D. Fast Growth of Carbon Nanotubes Using a Microwave Oven. *Carbon* **2015**, *82*, 327–336. [[CrossRef](#)]
179. Hsin, Y.-L.; Lin, C.-F.; Liang, Y.-C.; Hwang, K.C.; Horng, J.-C.; Ho, J.A.; Lin, C.-C.; Hwu, J.R. Microwave Arcing Induced Formation and Growth Mechanisms of Core/Shell Metal/Carbon Nanoparticles in Organic Solutions: Formation and Growth Mechanisms of Core/Shell Nanoparticles. *Adv. Funct. Mater.* **2008**, *18*, 2048–2056. [[CrossRef](#)]
180. Liu, Z.; Wang, J.; Kushvaha, V.; Poyraz, S.; Tippur, H.; Park, S.; Kim, M.; Liu, Y.; Bar, J.; Chen, H.; et al. Poptube Approach for Ultrafast Carbon Nanotube Growth. *Chem. Commun.* **2011**, *47*, 9912. [[CrossRef](#)]
181. Takagi, Y.; Tauchi, L.; Nguyen-Tran, H.-D.; Ohta, T.; Shimizu, M.; Ohta, K. Development of a Novel Method to Synthesize Carbon Nanotubes from Granulated Polystyrene and Nickel Nanoparticles by Microwave Heating. *J. Mater. Chem.* **2011**, *21*, 14569. [[CrossRef](#)]
182. Plonska-Brzezinska, M.E.; Palkar, A.; Winkler, K.; Echegoyen, L. Electrochemical Properties of Small Carbon Nano-Onion Films. *Electrochem. Solid-State Lett.* **2010**, *13*, K35. [[CrossRef](#)]
183. Mombeshora, E.T.; Nyamori, V.O. A review on the use of carbon nanostructured materials in electrochemical capacitors. *Int. J. Energy Res.* **2015**, *39*, 1955–1980. [[CrossRef](#)]
184. Bushueva, E.G.; Galkin, P.S.; Okotrub, A.V.; Bulusheva, L.G.; Gavrilo, N.N.; Kuznetsov, V.L.; Moiseev, S.I. Double Layer Supercapacitor Properties of Onion-like Carbon Materials. *Phys. Status Solidi B* **2008**, *245*, 2296–2299. [[CrossRef](#)]
185. Kumar, R.; Singh, R.K.; Alafedov, A.V.; Moshkalev, S.A. Rapid and Controllable Synthesis of Fe₃O₄ Octahedral Nanocrystals Embedded-Reduced Graphene Oxide Using Microwave Irradiation for High Performance Lithium-Ion Batteries. *Electrochim. Acta* **2018**, *281*, 78–87. [[CrossRef](#)]
186. Li, S.; Guo, C.; Qiao, Y. Microwave-Assisted Synthesis of Functionalized Graphene Hydrogels for High Performance Supercapacitors. *Mater. Sci. Eng. B* **2021**, *273*, 115407. [[CrossRef](#)]
187. Rosli, N.H.A.; Lau, K.S.; Winie, T.; Chin, S.X.; Chia, C.H. Synergistic Effect of Sulfur-Doped Reduced Graphene Oxide Created via Microwave-Assisted Synthesis for Supercapacitor Applications. *Diam. Relat. Mater.* **2021**, *120*, 108696. [[CrossRef](#)]
188. Ma, J.; Yamamoto, Y.; Su, C.; Badhulika, S.; Fukuhara, C.; Kong, C.Y. One-Pot Microwave-Assisted Synthesis of Porous Reduced Graphene Oxide as an Electrode Material for High Capacitance Supercapacitor. *Electrochim. Acta* **2021**, *386*, 138439. [[CrossRef](#)]
189. Kim, T.; Hyun, C.K.; Tung, T.T.; Lee, D.J.; Kim, H.; Woo, S.Y.; Yoon, H.G.; Suh, K.S. Ionic Liquid-Assisted Microwave Reduction of Graphite Oxide for Supercapacitors. *RSC Adv.* **2012**, *2*, 8808. [[CrossRef](#)]
190. Li, J.; Tang, Y.; Jin, R.; Meng, Q.; Chen, Y.; Long, X.; Wang, L.; Guo, H.; Zhang, S. Ultrasonic-Microwave Assisted Synthesis of GO/g-C₃N₄ Composites for Efficient Photocatalytic H₂ Evolution. *Solid State Sci.* **2019**, *97*, 105990. [[CrossRef](#)]
191. Lei, H.; Wang, Y.; Huo, J. Porous Graphitic Carbon Materials Prepared from Cornstarch with the Assistance of Microwave Irradiation. *Microporous Mesoporous Mater.* **2015**, *210*, 39–45. [[CrossRef](#)]
192. Wang, W.; Jin, J.; Wu, Y.; Zhang, W.; Jiang, H.; Li, X.; Wang, G. Unique Holey Graphene/Carbon Dots Frameworks by Microwave-Initiated Chain Reduction for High-Performance Compressible Supercapacitors and Reusable Oil/Water Separation. *J. Mater. Chem. A* **2019**, *7*, 22054–22062. [[CrossRef](#)]
193. Jessl, S.; Copic, D.; Engelke, S.; Ahmad, S.; De Volder, M. Hydrothermal Coating of Patterned Carbon Nanotube Forest for Structured Lithium-Ion Battery Electrodes. *Small* **2019**, *15*, 1901201. [[CrossRef](#)] [[PubMed](#)]

194. Sun, Y.; Du, X.; Zhang, J.; Huang, N.; Yang, L.; Sun, X. Microwave-Assisted Preparation and Improvement Mechanism of Carbon nanotube@NiMn₂O₄ Core-Shell Nanocomposite for High Performance Asymmetric Supercapacitors. *J. Power Sources* **2020**, *473*, 228609. [CrossRef]
195. Xu, Z.; Li, Z.; Tan, X.; Holt, C.M.B.; Zhang, L.; Amirkhiz, B.S.; Mitlin, D. Supercapacitive Carbon Nanotube-Cobalt Molybdate Nanocomposites Prepared via Solvent-Free Microwave Synthesis. *RSC Adv.* **2012**, *2*, 2753. [CrossRef]
196. Zheng, Y.; Tian, Y.; Liu, S.; Tan, X.; Wang, S.; Guo, Q.; Luo, J.; Li, Z. One-Step Microwave Synthesis of NiO/NiS@CNT Nanocomposites for High-Cycling-Stability Supercapacitors. *J. Alloys Compd.* **2019**, *806*, 170–179. [CrossRef]
197. Wang, Y.; Zhang, W.; Guo, X.; Liu, Y.; Zheng, Y.; Zhang, M.; Li, R.; Peng, Z.; Zhang, Y.; Zhang, T. One-Step Microwave-Hydrothermal Preparation of NiS/rGO Hybrid for High-Performance Symmetric Solid-State Supercapacitor. *Appl. Surf. Sci.* **2020**, *514*, 146080. [CrossRef]
198. Bae, S.-H.; Karthikeyan, K.; Lee, Y.-S.; Oh, I.-K. Microwave Self-Assembly of 3D Graphene-Carbon Nanotube-Nickel Nanostructure for High Capacity Anode Material in Lithium Ion Battery. *Carbon* **2013**, *64*, 527–536. [CrossRef]
199. Kumar, R.; Youssry, S.M.; Soe, H.M.; Abdel-Galeil, M.M.; Kawamura, G.; Matsuda, A. Honeycomb-like Open-Edged Reduced-Graphene-Oxide-Enclosed Transition Metal Oxides (NiO/CO₃O₄) as Improved Electrode Materials for High-Performance Supercapacitor. *J. Energy Storage* **2020**, *30*, 101539. [CrossRef]
200. Fang, J.; Li, M.; Li, Q.; Zhang, W.; Shou, Q.; Liu, F.; Zhang, X.; Cheng, J. Microwave-Assisted Synthesis of CoAl-Layered Double Hydroxide/Graphene Oxide Composite and Its Application in Supercapacitors. *Electrochim. Acta* **2012**, *85*, 248–255. [CrossRef]
201. Li, M.; Cheng, J.P.; Fang, J.H.; Yang, Y.; Liu, F.; Zhang, X.B. NiAl-Layered Double Hydroxide/Reduced Graphene Oxide Composite: Microwave-Assisted Synthesis and Supercapacitive Properties. *Electrochim. Acta* **2014**, *134*, 309–318. [CrossRef]
202. Liu, T.; Chai, H.; Jia, D.; Su, Y.; Wang, T.; Zhou, W. Rapid Microwave-Assisted Synthesis of Mesoporous NiMoO₄ Nanorod/Reduced Graphene Oxide Composites for High-Performance Supercapacitors. *Electrochim. Acta* **2015**, *180*, 998–1006. [CrossRef]
203. Reddy, B.J.; Vickraman, P.; Justin, A.S. Asymmetric Supercapacitor Device Performance Based on Microwave Synthesis of N-Doped Graphene/Nickel Sulfide Nanocomposite. *J. Mater. Sci.* **2019**, *54*, 6361–6373. [CrossRef]
204. Kumar, R.; Abdel-Galeil, M.M.; Ya, K.Z.; Fujita, K.; Tan, W.K.; Matsuda, A. Facile and Fast Microwave-Assisted Formation of Reduced Graphene Oxide-Wrapped Manganese Cobaltite Ternary Hybrids as Improved Supercapacitor Electrode Material. *Appl. Surf. Sci.* **2019**, *481*, 296–306. [CrossRef]
205. Nagaraju, P.; Arivanandhan, M.; Alsalmeh, A.; Alghamdi, A.; Jayavel, R. Enhanced Electrochemical Performance of α -MoO₃/Graphene Nanocomposites Prepared by an in Situ Microwave Irradiation Technique for Energy Storage Applications. *RSC Adv.* **2020**, *10*, 22836–22847. [CrossRef] [PubMed]
206. Miao, C.; Yin, X.; Xia, G.; Zhu, K.; Ye, K.; Wang, Q.; Yan, J.; Cao, D.; Wang, G. Facile Microwave-Assisted Synthesis of Cobalt Diselenide/Reduced Graphene Oxide Composite for High-Performance Supercapacitors. *Appl. Surf. Sci.* **2021**, *543*, 148811. [CrossRef]
207. Sridhar, V.; Park, H. Manganese Nitride Stabilized on Reduced Graphene Oxide Substrate for High Performance Sodium Ion Batteries, Super-Capacitors and EMI Shielding. *J. Alloys Compd.* **2019**, *808*, 151748. [CrossRef]
208. Vimuna, V.M.; Athira, A.R.; Dinesh Babu, K.V.; Xavier, T.S. Simultaneous Stirring and Microwave Assisted Synthesis of Nanoflakes MnO₂/rGO Composite Electrode Material for Symmetric Supercapacitor with Enhanced Electrochemical Performance. *Diam. Relat. Mater.* **2020**, *110*, 108129. [CrossRef]
209. Kumar, R.; Savu, R.; Singh, R.K.; Joanni, E.; Singh, D.P.; Tiwari, V.S.; Vaz, A.R.; da Silva, E.T.S.G.; Maluta, J.R.; Kubota, L.T.; et al. Controlled Density of Defects Assisted Perforated Structure in Reduced Graphene Oxide Nanosheets-Palladium Hybrids for Enhanced Ethanol Electro-Oxidation. *Carbon* **2017**, *117*, 137–146. [CrossRef]
210. Ma, T.; Liu, H.; Wang, Y.; Zhang, M. Rapid Construction of Three-Dimensional Sulfur Doped Graphene Supported by NiFeS₂ Interconnected Networks as Convenient Electron/Ion Transport Channels for Flexible Supercapacitors. *Electrochim. Acta* **2019**, *309*, 1–10. [CrossRef]
211. Kumar, R.; Oh, J.-H.; Kim, H.-J.; Jung, J.-H.; Jung, C.-H.; Hong, W.G.; Kim, H.-J.; Park, J.-Y.; Oh, I.-K. Nanohole-Structured and Palladium-Embedded 3D Porous Graphene for Ultrahigh Hydrogen Storage and CO Oxidation Multifunctionalities. *ACS Nano* **2015**, *9*, 7343–7351. [CrossRef]
212. Khamlich, S.; Mokrani, T.; Dhalmi, M.S.; Mothudi, B.M.; Maaza, M. Microwave-Assisted Synthesis of Simonkolleite Nanoplatelets on Nickel Foam-Graphene with Enhanced Surface Area for High-Performance Supercapacitors. *J. Colloid Interface Sci.* **2016**, *461*, 154–161. [CrossRef] [PubMed]
213. Zhao, F.; Xie, D.; Huang, W.; Song, X.; Aurang Zeb Gul Sial, M.; Wu, H.; Deng, F.; Zhang, Q.; Zou, J.; Zeng, X. Defect-Rich Honeycomb-like Nickel Cobalt Sulfides on Graphene through Rapid Microwave-Induced Synthesis for Ultrahigh Rate Supercapacitors. *J. Colloid Interface Sci.* **2020**, *580*, 160–170. [CrossRef] [PubMed]
214. Sridhar, V.; Kim, H.-J.; Jung, J.-H.; Lee, C.; Park, S.; Oh, I.-K. Defect-Engineered Three-Dimensional Graphene-Nanotube-Palladium Nanostructures with Ultrahigh Capacitance. *ACS Nano* **2012**, *6*, 10562–10570. [CrossRef] [PubMed]
215. Lee, J.-S.M.; Briggs, M.E.; Hu, C.-C.; Cooper, A.I. Controlling Electric Double-Layer Capacitance and Pseudocapacitance in Heteroatom-Doped Carbons Derived from Hypercrosslinked Microporous Polymers. *Nano Energy* **2018**, *46*, 277–289. [CrossRef]
216. Lim, E.; Jo, C.; Lee, J. A Mini Review of Designed Mesoporous Materials for Energy-Storage Applications: From Electric Double-Layer Capacitors to Hybrid Supercapacitors. *Nanoscale* **2016**, *8*, 7827–7833. [CrossRef]

217. Fan, L.-Q.; Zhong, J.; Wu, J.-H.; Lin, J.-M.; Huang, Y.-F. Improving the Energy Density of Quasi-Solid-State Electric Double-Layer Capacitors by Introducing Redox Additives into Gel Polymer Electrolytes. *J. Mater. Chem. A* **2014**, *2*, 9011. [[CrossRef](#)]
218. Ali, M.; Riaz, R.; Anjum, A.S.; Sun, K.C.; Li, H.; Ahn, S.; Jeong, S.H.; Ko, M.J. Microwave-Assisted Ultrafast in-Situ Growth of N-Doped Carbon Quantum Dots on Multiwalled Carbon Nanotubes as an Efficient Electrocatalyst for Photovoltaics. *J. Colloid Interface Sci.* **2021**, *586*, 349–361. [[CrossRef](#)]
219. Saumya, K.; Naskar, S.; Mukhopadhyay, T. ‘Magic’ of Twisted Multi-Layered Graphene and 2D Nano-Heterostructures. *Nano Futur.* **2023**, *7*, 032005. [[CrossRef](#)]
220. Zhong, Y.; Zhen, Z.; Zhu, H. Graphene: Fundamental Research and Potential Applications. *FlatChem* **2017**, *4*, 20–32. [[CrossRef](#)]
221. Borges-Vilches, J.; Figueroa, T.; Guajardo, S.; Meléndrez, M.; Fernández, K. Development of Gelatin Aerogels Reinforced with Graphene Oxide by Microwave-Assisted Synthesis: Influence of the Synthesis Conditions on Their Physicochemical Properties. *Polymer* **2020**, *208*, 122951. [[CrossRef](#)]
222. Tung, T.T.; Pereira, A.L.C.; Poloni, E.; Dang, M.N.; Wang, J.; Le, T.-S.D.; Kim, Y.-J.; Pho, Q.H.; Nine, M.J.; Shearer, C.J.; et al. Irradiation Methods for Engineering of Graphene Related Two-Dimensional Materials. *Appl. Phys. Rev.* **2023**, *10*, 031309. [[CrossRef](#)]
223. Cuenca, J.A.; Thomas, E.; Mandal, S.; Williams, O.; Porch, A. Microwave Determination of Sp² Carbon Fraction in Nanodiamond Powders. *Carbon* **2015**, *81*, 174–178. [[CrossRef](#)]
224. Adam, M.; Hart, A.; Stevens, L.A.; Wood, J.; Robinson, J.P.; Rigby, S.P. Microwave Synthesis of Carbon Onions in Fractal Aggregates Using Heavy Oil as a Precursor. *Carbon* **2018**, *138*, 427–435. [[CrossRef](#)]
225. Ahmed, G.H.G.; Laiño, R.B.; Calzón, J.A.G.; García, M.E.D. Facile Synthesis of Water-Soluble Carbon Nano-Onions under Alkaline Conditions. *Beilstein J. Nanotechnol.* **2016**, *7*, 758–766. [[CrossRef](#)] [[PubMed](#)]
226. Vadahanambi, S.; Jung, J.-H.; Kumar, R.; Kim, H.-J.; Oh, I.-K. An Ionic Liquid-Assisted Method for Splitting Carbon Nanotubes to Produce Graphene Nano-Ribbons by Microwave Radiation. *Carbon* **2013**, *53*, 391–398. [[CrossRef](#)]
227. Qureshi, S.S.; Shah, V.; Nizamuddin, S.; Mubarak, N.M.; Karri, R.R.; Dehghani, M.H.; Ramesh, S.; Khalid, M.; Rahman, M.E. Microwave-Assisted Synthesis of Carbon Nanotubes for the Removal of Toxic Cationic Dyes from Textile Wastewater. *J. Mol. Liq.* **2022**, *356*, 119045. [[CrossRef](#)]
228. Chakraborty, S.; Simon, R.; Vadakkekara, A.; Mary, N.L. Microwave Assisted Synthesis of Poly(Ortho-Phenylenediamine-Co-Aniline) and Functionalised Carbon Nanotube Nanocomposites for Fabric-Based Supercapacitors. *Electrochim. Acta* **2022**, *403*, 139678. [[CrossRef](#)]
229. Kumar, R.; Singh, R.K.; Tiwari, V.S.; Yadav, A.; Savu, R.; Vaz, A.R.; Moshkalev, S.A. Enhanced Magnetic Performance of Iron Oxide Nanoparticles Anchored Pristine/N-Doped Multi-Walled Carbon Nanotubes by Microwave-Assisted Approach. *J. Alloys Compd.* **2017**, *695*, 1793–1801. [[CrossRef](#)]
230. Kumar, R.; da Silva, E.T.S.G.; Singh, R.K.; Savu, R.; Alaferdov, A.V.; Fonseca, L.C.; Carossi, L.C.; Singh, A.; Khandka, S.; Kar, K.K.; et al. Microwave-Assisted Synthesis of Palladium Nanoparticles Intercalated Nitrogen Doped Reduced Graphene Oxide and Their Electrocatalytic Activity for Direct-Ethanol Fuel Cells. *J. Colloid Interface Sci.* **2018**, *515*, 160–171. [[CrossRef](#)]
231. Kumar, R.; Singh, R.K.; Savu, R.; Dubey, P.K.; Kumar, P.; Moshkalev, S.A. Microwave-Assisted Synthesis of Void-Induced Graphene-Wrapped Nickel Oxide Hybrids for Supercapacitor Applications. *RSC Adv.* **2016**, *6*, 26612–26620. [[CrossRef](#)]
232. Kumar, R.; Youssry, S.M.; Joanni, E.; Sahoo, S.; Kawamura, G.; Matsuda, A. Microwave-Assisted Synthesis of Iron Oxide Homogeneously Dispersed on Reduced Graphene Oxide for High-Performance Supercapacitor Electrodes. *J. Energy Storage* **2022**, *56*, 105896. [[CrossRef](#)]
233. Yang, S.; Li, S.; Song, L.; Lv, Y.; Duan, Z.; Li, C.; Praeg, R.F.; Gao, D.; Chen, G. Defect-Density Control of Platinum-Based Nanoframes with High-Index Facets for Enhanced Electrochemical Properties. *Nano Res.* **2019**, *12*, 2881–2888. [[CrossRef](#)]
234. Lu, J.; Luo, L.; Yin, S.; Hasan, S.W.; Tsiakaras, P. Oxygen Reduction Reaction over PtFeM (M = Mo, V, W) Alloy Electrocatalysts: Role of the Compressive Strain Effect on Pt. *ACS Sustain. Chem. Eng.* **2019**, *7*, 16209–16214. [[CrossRef](#)]
235. Luo, M.; Zhao, Z.; Zhang, Y.; Sun, Y.; Xing, Y.; Lv, F.; Yang, Y.; Zhang, X.; Hwang, S.; Qin, Y.; et al. PdMo Bimetallic for Oxygen Reduction Catalysis. *Nature* **2019**, *574*, 81–85. [[CrossRef](#)] [[PubMed](#)]
236. Back, S.; Kim, J.-H.; Kim, Y.-T.; Jung, Y. Bifunctional Interface of Au and Cu for Improved CO₂ Electroreduction. *ACS Appl. Mater. Interfaces* **2016**, *8*, 23022–23027. [[CrossRef](#)] [[PubMed](#)]
237. Rondinini, S.; Aricci, G.; Krpetić, Ž.; Locatelli, C.; Minguzzi, A.; Porta, F.; Vertova, A. Electroreductions on Silver-Based Electrocatalysts: The Use of Ag Nanoparticles for CHCl₃ to CH₄ Conversion. *Fuel Cells* **2009**, *9*, 253–263. [[CrossRef](#)]
238. Wang, Y.; Zhang, L.; Yin, K.; Zhang, J.; Gao, H.; Liu, N.; Peng, Z.; Zhang, Z. Nanoporous Iridium-Based Alloy Nanowires as Highly Efficient Electrocatalysts Toward Acidic Oxygen Evolution Reaction. *ACS Appl. Mater. Interfaces* **2019**, *11*, 39728–39736. [[CrossRef](#)]
239. Zhu, J.; Chen, Z.; Xie, M.; Lyu, Z.; Chi, M.; Mavrikakis, M.; Jin, W.; Xia, Y. Iridium-Based Cubic Nanocages with 1.1-Nm-Thick Walls: A Highly Efficient and Durable Electrocatalyst for Water Oxidation in an Acidic Medium. *Angew. Chem. Int. Ed.* **2019**, *58*, 7244–7248. [[CrossRef](#)]
240. Liu, X.; Dai, L. Carbon-Based Metal-Free Catalysts. *Nat. Rev. Mater.* **2016**, *1*, 16064. [[CrossRef](#)]

Disclaimer/Publisher’s Note: The statements, opinions and data contained in all publications are solely those of the individual author(s) and contributor(s) and not of MDPI and/or the editor(s). MDPI and/or the editor(s) disclaim responsibility for any injury to people or property resulting from any ideas, methods, instructions or products referred to in the content.